ABSTRACT

BHANUSHALI, HARDIK VASANT. Investigation of the Mechanical Properties of Woven Glass Fiber Composites with Inter-laminar Aligned Carbon Nanotube Sheets. (Under the direction of Dr. Philip Bradford.)

This investigation describes the thermal chemical vapor deposition (CVD) process used to synthesize drawable multi-walled carbon nanotube (MWCNT) array followed by the design, fabrication and testing of woven glass fiber reinforced epoxy matrix laminates with aligned CNT sheets integrated into the bulk composite in order to improve the matrix dominated through thickness properties like interlaminar fracture toughness at ply interfaces. The Mode I and Mode II interlaminar fracture toughness of various CNT modified samples were investigated using double cantilever beam (DCB) and end notched flexure (ENF) experiments respectively. Short beam strength (SBS) and in-plane mechanical properties of the CNT modified samples were also investigated using SBS and Tensile experiments respectively.

Moderate improvement was observed in Mode I and Mode II fracture toughness at crack initiation when aligned CNT sheets with a basis weight of 0.354 g/m^2 were used to modify the ply interface. Significant reduction in the above stated properties was experienced in case of using of aligned CNT sheets with a basis weight of 0.708 g/m^2 and 1.41 g/m^2. No compromise in the in-plane mechanical properties of the laminate was seen and very little improvement is observed in the shear related short beam strength of the CNT modified laminates as compared to the control samples. Integration of aligned CNT sheets into the composite laminate imparted in-plane and through thickness electrical properties into the non-conductive glass fiber reinforced epoxy composite laminates. The enhancement in the

through thickness properties was attributed to CNT crack bridging, fracture and pullout along with them partly reinforcing the fiber matrix interface and hence toughening it.

Investigation of the Mechanical Properties of Woven Glass Fiber Composites with Inter-laminar Aligned Carbon Nanotube Sheets

by
Hardik Vasant Bhanushali

A thesis submitted to the Graduate Faculty of
North Carolina State University
in partial fulfillment of the
requirements for the degree of
Master of Science

Textile Engineering

Raleigh, North Carolina

2013

APPROVED BY:

_____	_____
Dr. Xiangwu Zhang	Dr. Kara Peters

_____
Dr. Philip Bradford
Chair of Advisory Committee

DEDICATION

This work is dedicated to my Pappa! (Dad): Late Shri Vasant Lalji Bhanushali.

BIOGRAPHY

Hardik Vasant Bhanushali was born in Mumbai, India on November 17, 1989 to Vasant and Priya Bhanushali. After graduating from Institute of Chemical Technology (previously known as University Department of Chemical Technology) with a Bachelor of Technology degree in Fiber and Textile Processing Technology in 2011, he enrolled at North Carolina State University to pursue a degree in Textile Engineering. From January 2012, Hardik began working on Carbon Nanotubes and their application in structural materials under the direction of Dr. Philip Bradford. After completing his Master's degree from North Carolina State University, he will start his career in the polymer composite industry.

ACKNOWLEDGEMENTS

This work was made possible with the support, guidance and help of many people. I would like to take this opportunity to thank my advisor, Dr. Philip Bradford for providing me with a chance to work under him and guiding me through this research. I am grateful to achieve his endless support and encouragement throughout my stay in NCSU.

I would like to thank my committee members: Dr. Xiangwu Zhang and Dr. Kara Peters for providing their help and guidance throughout this work. I would also like to thank Dr. Abdel-Fattah Mohamed Seyam and Dr. Trevor Little for allowing me to use their equipments.

I am also thankful to all my lab members. Kelly, Can and Ozkan, thank you for mentoring me at the start of my research career and guiding me throughout. James and Shagayegh, you guys were great lab mates. Murphy, Kun, Omar, Spencer, Ang and Rachel; you guys were an awesome company.

There were several individuals whose timely assistance made this work possible. I would like to thank Rahul Vallabh, Tri Vu, Teresa White, Jan Ballard and Judy Elson for training me on various equipments and extending their help as and when required. I would also like to thank Sibei Xia for always helping me cut my prepreg fabrics on short notice.

Special thanks to Anurag, Nitish, Prithwish, Kushal and Krisha for helping me in every possible way during my thesis-writing days and motivating me throughout.

Finally, I would like to thank my family, especially my Mom. None of this would have been possible without your unconditional love and support. I love you.

TABLE OF CONTENTS

LIST OF TABLES

LIST OF FIGURES

Chapter 1 Introduction

Fiber reinforced composites have seen an increasing role in automotive, aerospace and marine industry due to their high specific strength, stiffness, light weight, better impact resistance and high durability. They are gaining attention as structural materials which can be designed with outstanding mechanical and physical properties. These features are achieved due to the excellent fiber dominated in-plane properties of composites which can be tailored according to the design requirements for any particular application. Composites can also be fabricated with directional control as per their end use but every added advantage come with an increased design complexity and challenging failure modes. Unlike their in-plane properties, the through thickness properties of composites such as delamination resistance are generally less than desired. These through thickness properties are governed by the matrix dominated interlaminar region and the relatively weak fiber matrix interface [1] whose properties are lower than the reinforced fiber by an order of 10-20. This leaves composites susceptible to out of plane damage which could occur by matrix cracking and interfacial failure leading to interlaminar delamination. Delamination, which is known as a life-limiting damage, severely reduces the overall in-plane compressive properties which render the composite unfit for certain load carrying structural applications. Interlaminar fracture toughness and interfacial shear strength between the fiber and matrix are thus the important parameters in monitoring the through thickness properties of the composites. Mechanical solutions such as stitching and z-pinning, changing the fiber architecture by braiding and 3D weaving, toughening the resins by incorporating toughening agents or thermoplastic binders

and interleaving has been developed to improve Interlaminar fracture toughness. However most of these developments results in compromising the in-plane mechanical properties; where stitching, braiding, 3D weaving and z-pinning reduce the overall in-plane properties, toughened resins and interleaving degrades the compressive strength of the composite. Micro and Nano sized fillers are also used to this effect. A limitation of these additives is the formation of large stress concentration around agglomerated fillers. Extensive research has been done on incorporating nano-particle fillers, as small as carbon nanotubes (CNTs) into the composite to achieve toughened resins and better through thickness properties without compromising the in-plane properties. CNTs have proven themselves effective in improving the matrix properties and in facilitating load transfer from the matrix to the fiber thus improving the fiber-matrix interface resulting in improved delamination resistance.

Owing to their small size, light-weight, extra-ordinary mechanical, electrical and thermal properties along with their large aspect ratio and higher specific surface area [2] CNTs have been used in various forms to impart multi-functionality to the composite materials. CNTs can be used as effective reinforcements and sensors simultaneously due to their exceptional strength, stiffness, failure strain along with their characteristic electrical response to the applied load [3][4][5][6]. CNTs have also been used to improve the thermal, electrical and mechanical properties of the resins as compared to the base polymer [7][8][9]. However, the CNTs properties are not utilized to its fullest due to its tendency to agglomerate within the polymer. Dispersing techniques like direct mixing, mechanical stirring, sonication and high shear mixing are therefore used to break the agglomerates and achieve uniform dispersion [10][11]. Improvements in through thickness properties have also been achieved

by directly growing the CNTs on the reinforced fiber [12][13]. Even though it has been proven an effective method for improving the through thickness properties, this process has a limitation on the type and the size of the reinforcement used.

This investigation is focused on processing the composite laminates by incorporating CNTs into them using a novel method which utilizes its beneficial properties, lowers the possibility of agglomeration and allows the incorporation of CNTs into any fiber-matrix system used. Uniform CNT placement throughout the laminate is achieved with active control over CNT location and 2D orientation. Chapter 4 will show a three step method which includes synthesizing a drawable multi-walled carbon nanotubes (MWCNT) arrays using CVD method, drawing the MWCNT array into aligned CNT sheets and placing them onto the woven glass fiber reinforced epoxy matrix prepreg plies followed by consolidating the layup using vacuum bagging and a hot press. CNT sheets with a basis weight of 0.354 g/m^2 were used to modify the prepreg plies before stacking and curing into laminate. The effectiveness of this method in improving the matrix related through thickness properties was evaluated by measuring the Mode I and Mode II interlaminar fracture toughness at crack initiation and short beam strength of the CNT modified composite laminate. Tensile testing was also done on CNT modified laminates to validate that in-plane mechanical properties were not compromised.

Chapter 2 Literature Review

2.1. Carbon Nanotubes

2.1.1. Structure and Properties

Carbon Nanotubes are nano-scale materials with unique physical, mechanical and remarkable electronic properties. They have a high aspect ratio and exhibit great strength, and stiffness. They can posses metal like electrical conductivity and in some cases they have thermal conductivity better than metals [14][15]. These properties combined with a very low density, makes them an attractive reinforcement in composite materials. This includes toughening polymer matrices as well as continuous fiber reinforced polymer composites.

With their application in many diverse fields of science ranging from macroscopic structural applications-composites, to nano-scale energy storage applications-lithium ion batteries, Carbon Nanotubes are considered the most exciting materials to work with in the 21^{st} century. Since their notable observation by Ijima in 1991 in the High Resolution – Transmission Electron Microscopy (HR-TEM) images of fullerene soot produced in an arc discharge [16], a new realm of research opportunities was opened, and a large amount of resources have been devoted to understanding their synthesis and use.

The carbon nanotube structure was explored by Ijima and others using HR-TEM and Scanning Tunneling Microscopy (STM) which confirmed that nanotubes are seamless cylinders derived from honeycomb lattice representing a single atomic layer of crystalline

graphite [17], called a graphene sheet. Hence the planar sp^2 bonding of graphite is expected to play a significant role in carbon nanotubes.

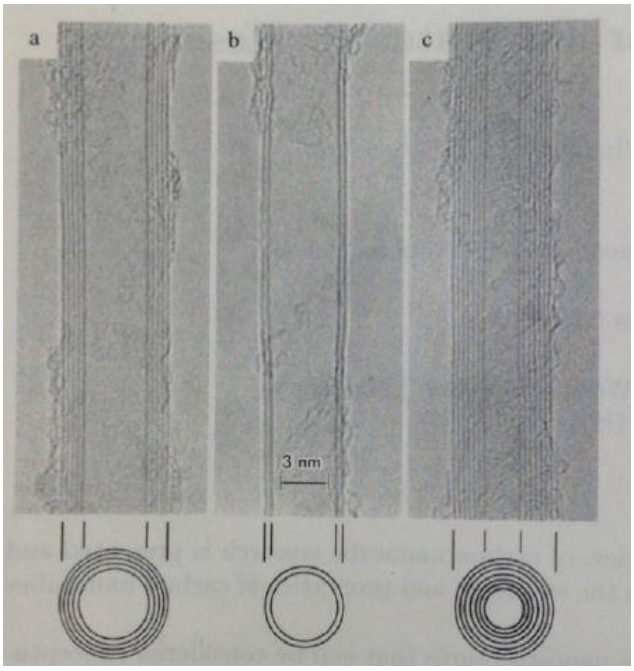

Figure 2-1: TEM Observation of multi-wall coaxial nanotubes reported by Ijima [16]

Owing to the carbon-carbon covalent sp^2 bonding and the highly regular and symmetric structural morphology, CNT's exhibit high anisotropy of their properties in their axial direction. A single graphene sheet rolled into a cylinder with the diameter on the order of 1 nanometer and length ranging from hundreds of microns to few centimeters is called a single-walled-carbon nanotube (SWCNT). Two sheets rolled concentrically are known as double-walled carbon nanotube (DWCNT), whereas multiple graphene sheets rolled into

concentric cylinders are called multi-walled carbon nanotubes (MWCNTs). The spacing between the concentric tubes is 0.34 nm, the same as interplanar spacing in graphite.

The curvature of the planar graphite sheet causes the rehybridization of a small amount of sp^2 orbitals towards sp^3 due to quantum confinement in the radial and circumferential directions [18]. SWCNT are also defined by the way the graphene sheet is rolled. It is characterized uniquely by a pair of integers (n,m) which specify the chiral vector $Ch = na_1 + ma_2$ which connects two crystallographically equivalent sites on a 2D graphene sheet and a chiral angle θ between the chiral vector and the zigzag direction (θ=0) []. Three distinct types of nanotubes can be generated by rolling the graphene sheet in to cylinder as follows; zigzag (θ=0), (n,0) and (0,m); armchair (θ=30) and (n,n) and chiral (0<θ<30) and (n,m). The chirality of the nanotube affects the conductance [19]. Armchair nanotubes are metallic whereas zigzag and chiral nanotubes are semi-conducting. Also if (n-m)/3 is an integer, SWCNTs will be metallic, else they will be semiconducting. In case of the availability of random values of the indices, based solely on geometry we expect two third of the nanotubes to be semi-conducting and the rest one third to be metallic. Determining the chirality of MWCNT is more complex due to the presence of multiple rolled sheets and their individual chiralities. MWCNT are generally a mixture of metallic and semiconducting tubes.

The higher surface energy and flexibility of SWCNT's usually causes them to agglomerate and form bundles of tens of individual SWCNT. They are held together by van der Waal's

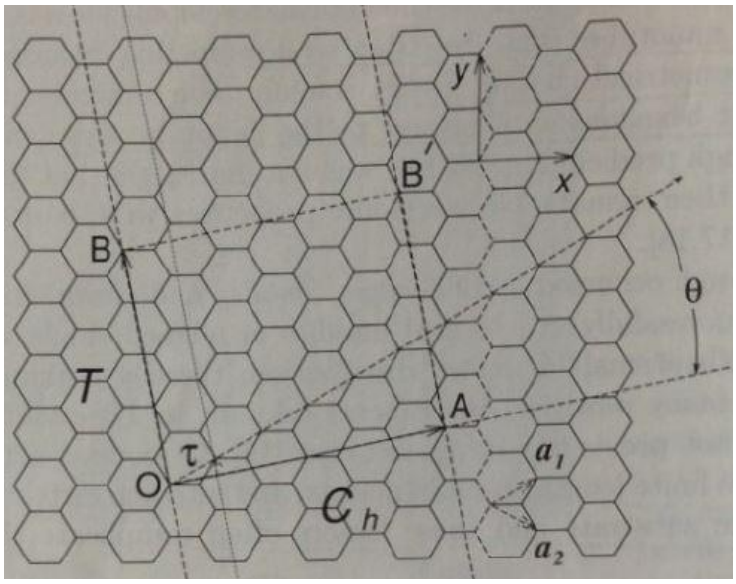

Figure 2-2: The chiral vector defined on the honeycomb lattice of carbon atoms by unit vectors a1 and a2 and the chiral angle θ with respect to the zigzag axis [19].

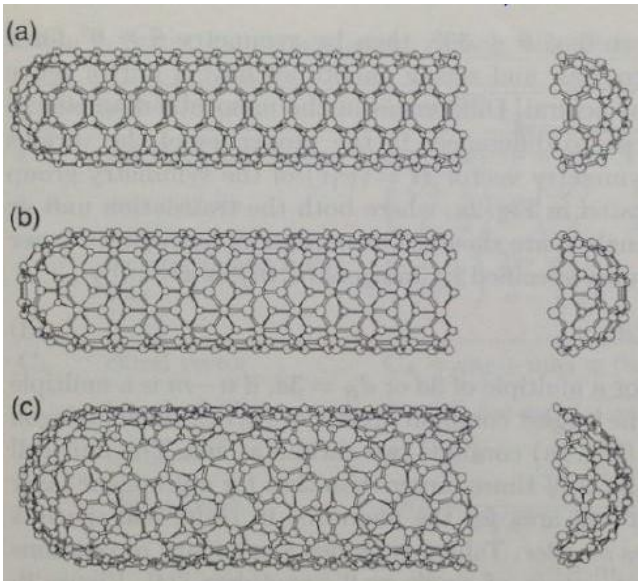

Figure 2-3: Schematic models for SWCNT (a) Armchair; (b) Zigzag and (c) General [19].

force and are very difficult to isolate and hence individual SWCNT's are rarely available to test.

Bundle properties are generally inferior then individual properties; hence the computational experiments were carried out using simulations by a researchers to obtain the elastic properties using the empirical force constant model assuming that elastic properties are not sensitive to radius and number of walls for SWCNT's and MWCNT's. Young's modulus and shear modulus were predicted to be about 1 TPa and 0.5 TP a respectively [20]. Similar results were reported by a group who treated the nested individual layers of MWCNT as single walled frame-like structures and simulated the properties by molecular structural mechanics method [21]. Young's modulus and shear modulus were reported to be 1.05 ± 0.05 Tpa and 0.4 ± 0.05 TPa respectively. Researchers have also probed into individual CNT's. Measuring the amplitude of intrinsic thermal vibrations of cantilevered cylindrical CNT's, under transmission electron microscopy, Young's Modulus was reported in the range of 0.4- 4.15 TPa with the mean of 1.8 TPa [22]. More realistic test results were obtained by performing direct tensile loading tests on arc-grown MWCNT's and SWCNT's. Tensile strengths were reported to be in the range of 11-63 GPa and the moduli was reported to be in the range of 270-950 GPa for individual MWCNT, whereas tensile strength of 13-52 GPa was reported for SWCNT and its moduli in the range of 320 to 1470 GPa [23]. CVD grown MWCNT's were measured with 20 times lower modulus values ranging of 12-50 GPa and the tensile strength was reported to be 4 GPa, confirming the sensitivity of elastic properties to the severity of defects and manufacturing techniques [24].

2.1.2. Carbon Nanotube Production

Arc-discharge and laser ablation methods have been used to synthesize high quality, near defect free CNT's in limited quantities, whereas catalytic chemical vapor deposition, CVD, is used to obtain higher yield and production of CNT's but with high defect densities. In all cases however, purification is required.

Carbon nanotubes were first observed on the negative end of carbon electrode in the carbon-soot made by arc discharge. In arc discharge, carbon atoms are evaporated by plasma of an inert gas ignited by high currents passed through opposing carbon anode and cathode. This method has been developed to produce high quality SWCNT's and MWCNT's. MWCNT's growth via arc discharge required control over growth conditions like the inert gas pressure in the discharging chamber, the cooling rate, plasma stability between two electrodes and the arcing current, whereas a metal catalyst is required in the arc-discharge system for producing SWCNT's. As an initial breakthrough in growing high quality CNT's by arc-discharge method, straight and highly crystalline MWCNT's with length on the order of tens of micron and diameters in the range of 5-30 nm were grown [25] and a carbon anode containing a small percentage of Cobalt catalyst was used in the discharge experiments to produce substantial amount of SWCNT's. One atomic percentage of yttrium and 4.2 atomic percentage of nickel were used in a carbon anode as metal catalysts to achieve optimized SWCNT growth using this method [26][27].

Laser ablation uses intense laser pulses to ablate a metal catalyst induced carbon/graphite material placed in a tube-furnace at high temperatures. Inert gas is flown

through the growth chamber during ablation to carry the grown nanotubes downstream to be collected on a cold finger. This method is mainly used to produce high quality SWCNT's. Ropes of tens of individual high quality SWCNT's closely packed into hexagonal crystals via van der Waals interaction were produced by pulsating intense laser on a carbon target containing 0.5 atomic percentage of nickel and cobalt at 1200^{o} C [28]. Researchers also have successfully harnessed solar energy; using a 2-kW solar furnace which consists of a flat tracking mirror that reflects the sunlight toward a parabolic mirror onto a graphite target; for producing SWCNT's [29].

Chemical vapor deposition has been successfully used in producing filaments and nanotube materials. It is used to transform gaseous reactants into solid materials in the form of thin films and powder and deposit them on a solid surface. It is mainly used to produce low cost multi-walled CNTs. This process consists of following steps: 1) Vaporization of the precursor molecules into a reactor; 2) Diffusion and adsorption of gaseous molecules on a substrate; 3) Decomposition and incorporation of the precursors into solid film and 4) Desorption of reaction products into gaseous phase [30]. CVD reactions are usually done in a temperature controlled quartz tube furnace at varied pressure range. Key parameters governing nanotube growth are hydrocarbons, catalysts and growth temperature [31]. Hydrocarbon precursors used for MWCNT growth are gases like ethylene [32], acetylene [33], cyclohexane [34] and benzene whereas methane and carbon monoxide are used for producing SWCNT [35]. Catalysts used generally are transition metal nanoparticles like Iron, Nickel, Cobalt and Molybdenum on support material such as alumina called as buffer, pre-deposited on metallic substrates like silica and stainless steel [31][32][36].

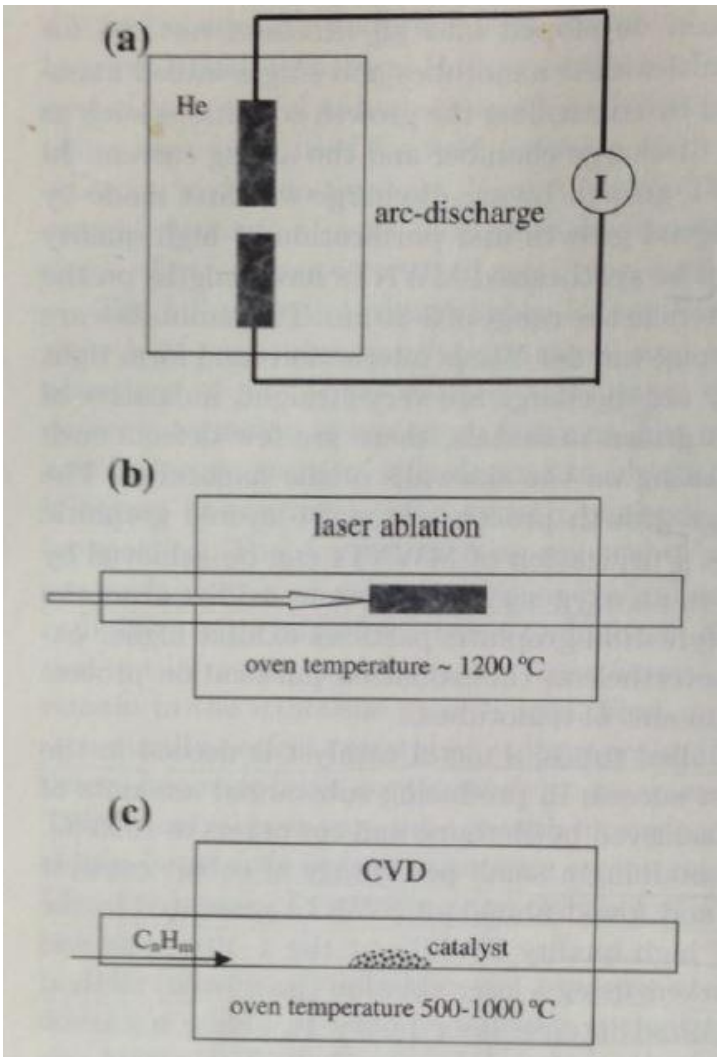

Figure 2-4: Schematic experimental setups for nanotubes growth methods [31]

Quartz is also being used as a substrate [37]. Temperature used for CVD growth is around 550^{o}C to 820^{o}C. Researchers have introduced water vapor in the CVD system during growth to sustain the growing process for a longer time and hence achieve taller arrays [32][38]. Work has also been done to replace the inconvenient catalyst deposition step by the introduction of floating catalyst. Super aligned CNT arrays have been synthesized with

higher yield and growth rates using floating catalyst and a quartz substrate. The CVD process has also been used to produce vertically aligned carbon nanotube arrays which can be later drawn into CNT yarns and CNT sheets [37].

2.1.3. Drawable vertically aligned CNT arrays

Vertically aligned CNT arrays are grown using thermal chemical vapor deposition (CVD) process on various metallic and quartz substrates with pre-deposited or floating catalysts. A general mechanism for CNT growth involves the dissociation of hydrocarbon molecules catalyzed by transition metals followed by dissolution and saturation of carbon atoms in metal nanoparticles. The precipitation of carbon from the saturated metal nanoparticles leads to the formation of carbon nanotubes [31]. It has been found that by the presence of van der Waals forces among multi-walled CNTs grown on a substrate, they can mutually support themselves by surrounding CNTs and self assemble into aligned structures [39]. This self assembling aligned orientation of CNTs involves the base growth method [39][40]. Porous silicon substrate with a patterned iron catalyst was used to achieve aligned nanotubes. Etching silicon wafers in hydrofluoric acid/methanol solution resulted into a thin nanoporous layer on the top of a macroporous silicon layer which produced a relatively narrow range of aligned nanotube diameters. Nanotube size distribution is seen to be affected by the catalyst particle size and its size distribution. By varying the CVD reaction time, height of the aligned CNT towers was controlled and could be produced in the range of 10-

240 μm. Other parameter which can significantly influence the growth is residence time which is controlled by the gas flow rate [39].

Although being efficient and in control, the above method involved too many preparation steps to produce a relatively short array height. CVD methods with one step growth have been developed for mass synthesis of ultralong vertically aligned MWCNTs [37].

This method has been the basis of synthesizing CNT arrays used in this investigation; hence we will delve deeper into the chloride mediated chemical vapor deposition for carbon nanotubes. CM-CVD eliminates the time involving steps like buffer and catalyst layer deposition and replaced the costly silicon substrate with quartz. It uses $FeCl_2$ powder as catalyst which evaporates around 550^o C and reacts with acetylene in the gaseous phase. Higher growth rate achieved was attributed to high dehydrogenation activity of iron chloride on acetylene, feature not seen with pre-deposited catalysts. Since $FeCl_2$ vaporizes and reacts in a gaseous phase, this method is used to coat the entire target surface. Acetylene is purged into the reactor at 10 Torr when the furnace temperature reaches 820^oC. Following reaction takes place inside the furnace:

$$FeCl_2 + C_2H_2 \rightarrow FeC_2 + 2HCl$$

Owing to low pressure and vapor phase reaction FeC_2 molecules and other carbon rich iron carbide clusters are formed which nucleate into nanoparticles on multiple gas phase collisions and get deposited on the quartz surface in the heated zone. Carbon has limited

solubility in the transition metals at high temperatures. On saturation, FeC_2 molecules segregate into graphene layers as follows:

$$FeC_2 \rightarrow FeC_{2-x} + xC$$

This reaction continues as acetylene reacts with iron chloride catalyst. These segregated graphene layers initiate CNT growth. Remaining $FeCl_2$ molecules are adsorbed at the base of CNTs, along with the chlorination of surface Fe atoms with HCl according to the following reaction:

$$Fe + 2HCl \rightarrow FeCl_2 + H_2$$

Acetylene is then decomposed on the CNT base after reacting with $FeCl_2$ using following reaction mechanism:

$$FeCl_2 + C_2H_2 \rightarrow FeC_2 + 2HCl$$

FeC_2 will then be segregated into graphene layers forming nanotubes by above mentioned reaction mechanism. This cycle is repeated continuously resulting into the growth of ultra-long CNTs in a very short time. A narrow size distribution of CNTs is achieved by flowing in consistent concentration of the carbon source gas throughout the process. Also these type of CNTs arrays are often easily drawn into CNT yarns by pulling CNTs out using tweezers.

Research has also been done to understand the optimum parameters and mechanism used to achieve Drawable CNT fiber from vertically aligned CNT forests []. Drawable and not drawable CNTs were observed in SEM and their in-situ drawing process was examined.

The root of the drawable CNTs was seen to be straight whereas that of not drawable CNTs was curly. This difference in the root was attributed to the lost activity of active catalyst particles due to amorphous carbon coating on them. This led to decreased number of CNTs and increased distance between individual CNT along with out of plane CNT synthesis. Because of the increased distance between the CNTs, very few or no bundles were seen attached to neighboring CNTs, leading to very few tangles in the CNT root. This was the primary reason of drawn CNTs from the top and middle being disconnected at the bottom and hence rendering the array not drawable. The reported draw-ability of the CNT yarns is attributed to the tangles, friction and van der Waals interactions between the CNTs which together provided the connection needed for drawing process. Other parameters influencing drawability were reported to be precise temperature range, gas flow rate and precursor concentration.

2.2. Composites:

Composite is a heterogeneous material made up of two or more homogeneous constituents that posses significantly different physical or chemical properties which remain separate and distinct. Properties of the composite materials are directly dependent and are determined by the properties of its constituents. Its constituents are divided into two major classes, one being stronger, stiffer, denser, rigid, the discontinuous phase called as the reinforcement and other being softer, ductile and lightweight, the continuous phase called as the matrix. This difference in its constituents can create anisotropy in composite which is

then engineered for the required application. It is also possible to design quasi-isotropic composites.

2.2.1. Types of Composites

Composites can be broadly classified into natural and engineered composites. There are numerous examples of naturally occurring composites like wood (cellulose fibers reinforced by lignin), bone (hydroxyapatite reinforced in collagen), insect exoskeleton, mollusk shell, nacre and many more. Natural composites tend to be weaker and less stiff than engineered ones but are often superior in terms of their design. Engineered composites are mainly divided into particle reinforced composites and fiber reinforced composites based on the size and type of the reinforcement used. Particulates are used as a reinforcing phase in particle reinforced composites whereas fibers are used as the reinforcing phase in fiber reinforced composites. Length to diameter ratio for particulates is approximately one and their dimensions may range from tens of nanometers to several millimeters. They are used as low cost fillers to increase hardness and toughness of the composite. Mostly ceramic particulates are used for their higher stiffness and strength. Fiber reinforced composites are further classified into discontinuous- short fiber composites and continuous fiber composites. Continuous fibers have a length to diameter ratio that approaches infinity and usually a diameter on the order of 10 micrometer.

2.2.2. Different Types of Fibers

A wide variety of fibers are available for use in composites and the number is ever increasing. Fibers are broadly divided into 5 types: Glass, Carbon, Polymeric, Ceramic and Nanofibers.

Glass: Owing to an appealing combination of good properties at low cost, glass fibers overall dominates as reinforcement in all, except for high-performance composite applications. Glass is an amorphous solid primarily made of Silicon and Oxygen with varying amounts of ionic metal oxide. Diameters of the individual fibers used in composite application vary between 10-20 micrometers. Different available glass compositions are E, S and C where E- stands for Electrical, S- for high Strength and C- for Corrosion resistant. Other notable advantages include good tolerance to high temperatures, radar transparency and higher toughness. Disadvantages include relatively low stiffness, moisture sensitivity, and abrasiveness.

Carbon: It has the highest strength and stiffness of all the available fibers with the ongoing rapid development towards new fibers with higher strength, stiffness and ultimate strain. It is made up of sp^2bonded carbon sheets aligned parallel to fiber axis. Fiber diameters vary in the range of 4-11 micrometer. They are manufactured from 3 different precursors namely: Rayon, Polyacrylonitrile (PAN) and petroleum pitch. The precursor used and the heat treatments employed during manufacturing dictate the end properties of carbon fiber. Notable advantages include tolerance to high temperatures and corrosive environments along with

lack of moisture sensitivity. Some disadvantages include their high price and lower toughness.

Polymeric Fibers: Frequently used polymeric fibers are Aramid (Kevlar) and high modulus Polyethylene. They are organic in nature. Polymeric fibers are not as popular composite reinforcements as glass and carbon. Different fibers are produced using different manufacturing methods and their properties could be varied by varying their molecular weight. Kevlar 29 has high toughness and is used in ballistic armor whereas the specific strengths and modulus of high molecular weight polyethylene is comparable to carbon fiber. Notable drawbacks include poor fiber-matrix compatibility and poor temperature tolerance.

Ceramic Fibers: Boron, SiC, and Al_2O_3 are the 3 main ceramic fibers. Used only for specialized applications where very high temperature tolerance is required, like refractory insulation, rocket nozzles, thermal protection, turbines etc. They are manufactured using CVD technique and sometimes use carbon fiber as their substrate. Boron fibers diameter is around 100 micrometer, whereas SiC has an approximate diameter around 140 micrometer. They have limited polymer-composite applications and are generally used in combination with metal and ceramic matrices. Silica fibers though are used in combination with polymer matrices in radomes and stealth aircraft due to their excellent di-electric properties.

Nanofibers: They are usually called whiskers. Whiskers have length to diameter ratio of order 10-1000 and diameters of order 0.1-1 micrometer. They are pure single crystals

manufactured through CVD. Whisker-reinforced materials are likely to be considered macroscopically isotropic.

2.2.3. Different types of Matrices

Matrix of a composite act as a binder that holds the reinforcement in place, protects it from external environmental effects, transfers the external loads to the reinforcement effectively, redistributes the load to surrounding fibers in case of fiber fracture and give them the required lateral support to prevent the fibers from buckling. Polymers, metals and ceramics are used as matrix materials and the corresponding composites are known as Polymer Matrix Composites (PMCs), Metal Matrix Composites (MMCs) and Ceramic Matrix Composites (CMCs). Here we will only look into PMCs. Polymer matrices are further subdivided into thermoplastics and thermosets.

Thermoplastic Polymers: Thermoplastics can soften upon heating, reshaped with the application of heat and pressure and reused. Poly-propylene, polyvinyl chloride, nylon, polyurethane, poly-ether-ether-ketone, polysulfone and polyphenylene sulfide are thermoplastic polymers which can be used as a matrix material for composites. They offer better potential for higher toughness and high volume low cost processing. Disadvantages include higher melt viscosity which makes it difficult for processing.

Thermosetting Polymers: Most frequently used thermoset polymer matrix materials are unsaturated polyesters, epoxies, vinylesters, phenolics and polyimides. Thermoset polymers

crosslink during fabrication forming a tightly bound 3-D network which will not melt given any amount of heat and hence they cannot be reshaped and reused.

Epoxies: Epoxies are primarily used in composites due to their improved toughness and temperature tolerance accompanied by low viscosity, low shrinkage and excellent fiber-matrix adhesion. A significant advantage with epoxy is that they can be partially cured and the crosslinking activity is seized by lowering the temperature; hence epoxy prepregs can be supplied. Disadvantage include high price, toxic emissions during processing and complex processing requirements at elevated temperatures and pressure which translates to costly manufacturing operations. Epoxies are characterized by temperature requirements during crosslinking. For example, room temperature epoxies crosslink at 25 deg Celcius in usually less than a day while high temperature epoxies may take days to gel at room temperature but can be fully cured in a matter of hours at high temperature.

2.2.4. Fiber Architecture Used

Composite properties strongly depend on the fiber architecture used as reinforcement. This encompasses variables such as fiber length, diameter, alignment, packing arrangement and their volume fraction. The most common reinforcement forms used in composites are as follows; 2-D nonwoven ‘Strand Mat’, A 2-D unidirectional prepreg, 2-D aligned fibers with binding yarns, Noncrimp/Stitched fabrics, Knitted fabrics, Braided fabrics and 2-D woven fabrics. Here we will look into 2-D woven fabric prepreg.

Pre-Impregnated 2-D woven fabrics: Yarns are weaved orthogonal to each other with one going alternately over and under successive orthogonal ones. The most common used weaves are plain weave, basket weave, twill weave and satin weave. Plain weave is the tightest possible weave pattern leading to higher crimp in the yarns whereas 8 harness satin weave has minimum interlacing and minimum crimp hence a very flexible weave is obtained with good drapeability. When a woven fabric is pre-impregnated with partially cured B-stage epoxy matrix, we get a 2-D woven prepreg. Depending on the type of epoxy used the shelf life can be from a few days to 12 months. Prepregs with a shelf life of a few days are stored in a freezer and thawed before usage.

2.2.5. Laminated composites

Laminated composites are made by stacking multiple plies or layers of the above described fiber architecture at different fiber orientations. Laminates are used to make high-performance composite components which can bear significant structural load in more than one direction. Laminate properties are governed by parameters like fiber orientation, number of plies, thickness and the stacking sequence. Laminates are defined by a short hand notation used to describe the stacking sequence. Lamination theory assumes that any individual layer is considered homogeneous, its properties can be isotropic, orthotropic or transversely isotropic and it will be perfectly bonded to the layers above and below it. Depending on the stacking sequence and geometry of individual plies, laminates are classified into symmetric, asymmetric, balanced, angle ply, cross-ply and quasi-isotropic laminates. Mechanical

properties of laminated composites are governed by three failure modes: Fiber failure, intra ply cracking and interlaminar matrix delamination. Although the in-plane properties of laminated composites largely depend on the reinforcements and their orientation, the through thickness transverse properties like interlaminar fracture toughness which represents delamination resistance, depend on the weak interface or the mechanical properties of the polymer matrix system [41] and are generally very low as compared to the in-plane properties. That makes laminates susceptible to delamination in the form of crack initiation and propagation in the laminar interfaces in various failure modes [42]. Delamination results from the interlaminar stresses generated by impacts, discontinuities in structure or from eccentricities in the structural load paths. It may also result from an improper curing cycle or the introduction of unwanted foreign bodies during manufacturing [43][44][45]. Fig. shows typical design details of some of the discontinuities causing delamination. Applied compressive force to a laminate can indirectly result in delamination by buckling and generating internal through thickness tensile and shear stresses. In many cases damage done by impacts will not even be seen on the surface. This type of damage is known as barely visible impact damage, which reduces the residual compressive strength of the impacted structure [46].In order to ensure the safety of laminated composites damage tolerant designs with higher safety factors are employed. This leads to an increase in structural weight of the composite along with an increased cost. Delamination is sub-critical failure mode which can severely affect the in-plane compressive properties of laminated composites by creating stiffness loss, local higher stress concentrations in plies and creating local instability leading

to the component's potential failure; hence is called as the life limiting damage growth mode [44][47].

Due to delamination's influence on the composite's structural integrity and performance, its causes should be avoided and methods for delaying and preventing delamination should be employed. Research is being done on delaying and preventing delamination and some of the approaches used are: improving layup design, improving the fiber architecture of the reinforcement (3D weaving, knitting, braiding), mechnically fastening the plies together (stitching, z-Pinning), developing new tougher resins, toughening the current resins, adhesive

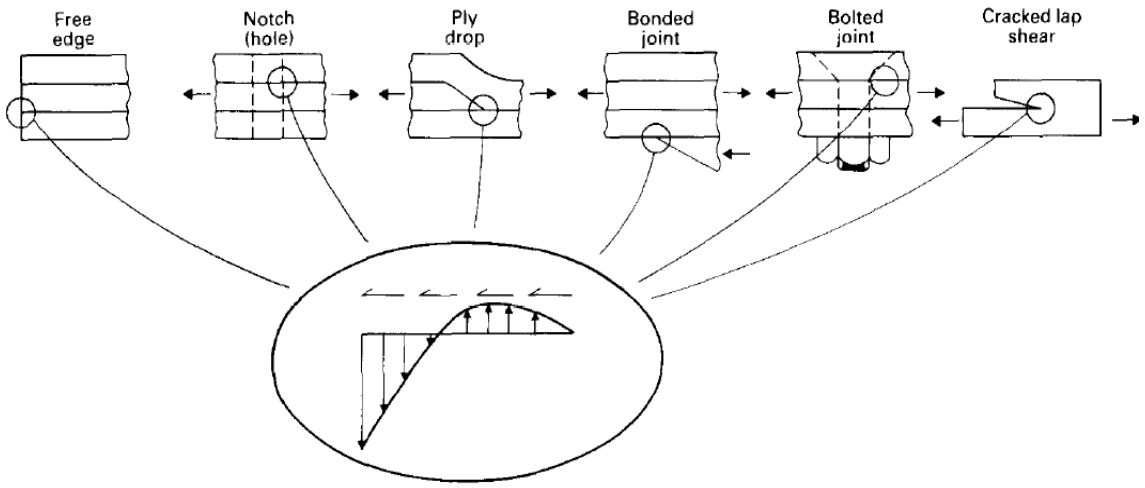

Figure 2-5: Source of out-of-plane loads from load path discontinuities [43].

interleaving and improving the fiber matrix interface properties. Here we will review some of the above mentioned techniques.

2.3. Methods used to improve Inter-laminar fracture toughness

2.3.1. Layup Design Considerations

Interlaminar stresses occur due to the mismatch in the engineering properties like poisson's ratio and co-efficient of mutual influence between the layers. Interface moment caused by the neighboring plies of different orientation also causes delamination. Interlaminar stresses are dependent on the stacking orientation of individual plies. It has been shown that angle plies ($\pm\theta$) generates interlaminar shear which could potentially lead to delamination; therefore one should avoid using angle plies together [48] and these plies should be interspersed between other plies. Other care which a designer should take is to keep the geometric discontinuities and free edges to the minimum. Since it is not always easy to reduce the free edges without affecting the properties, it is suggested to reinforce the free edges with fiber glass cloth [43][49]. It either prevents or considerably delays the edge delamination. Introducing the regions of high and low axial stiffness discreetly also helps preventing delamination from impact damage [43].

2.3.2. Toughening brittle resins

Inherently brittle thermoset matrices which have strain to failure of 2-3 % have been toughened by adding thermoplastic polymer to the uncured thermoset. ~0.1-0.5% of liquid rubber (carboxy terminated butadiene nitrile, CTBN) was added to uncured epoxy [50] to toughen the system. Phase separated, finely dispersed rubber was found chemically bonded to epoxy which improved the fracture toughness of the system. The effect of

polyurethane on Mode I and Mode II interlaminar fracture toughness of glass fiber reinforced epoxy matrix has also been studied. Addition of 15% polyurethane in the epoxy system resulted in 17% and 120% rise in the Mode I and Mode II interlaminar fracture toughness [51]. The degree of matrix toughening is governed by parameters like particle size, volume fraction and the size distribution. Shear deformation, dilation, arresting crack propogation, crazing and rubber tear are the mechanisms which toughens the brittle system [52]. The disadvantage of using this system is the reduced hot/wet performance of the composite limiting their use in primary structures.

2.3.3. z-Pinning

Techniques like 3D weaving, stitching and braiding have proven effective in reinforcing polymer laminate composites in the through thickness direction to improve the through thickness mechanical properties, delamination resistance, impact damage tolerance and in some cases even ultimate strength has been improved; However these reinforcements are suitable only for a dry fabric perform. Any attempts done to reinforce the uncured prepreg by the above mentioned techniques results in significant fiber damage which in turn affects the in-plane mechanical properties. Z-pinning is a simple, fast, effective and only available technique which can reinforce prepreg laminates in the through thickness direction and achieve better delamination resistance, impact damage tolerance and joint strength of prepreg laminates [53]. Ultrasonically assisted Z- fiber^{TM} (UAZ) process developed by Aztek Inc. [54] is the most common process used for z-pinning of laminates. Z-pins are made using high stiffness, high strength materials like steel, titanium or carbon composites. Their

diameter is of the order 0.2-1.0 mm. 0.5-4.0 volume % of z-pins are enough to enhance the through thickness properties of the composite significantly. A significant amount of research has been done to understand the delamination properties and interlaminar toughening mechanisms of z-pinned laminates. It is seen that z-Pinning is not effective at preventing shorter delamination cracks (below 2mm) but is very effective in resisting the propogation of longer cracks (above 2-5 mm) and it increases the interlaminar toughness of long cracks under modes I, II and mixed I/II loads [55][56]. Toughness value rise is seen to be linearly proportional to the volume % of z-Pins in the composite where the rise in mode I values is seen to be doubling for every 0.5% increase in the pin content, a modest increase is seen for mode II delamination toughness values [53][57]. z-Pinning has also proven effective at slowing down and stabilizing the delamination crack growth under mode I fatigue loading. z-Pinning toughens the interlaminar region under mode I loading by elastic deformation, debonding and frictional pull out of z-pins [56], whereas, elastic shear deformation, debonding, snubbing and shear induced pull-outs of z-pins are used to toughen the composite from delamination under mode II load. Finite Element Analysis of z-pinned laminates has predicted a rapid increase in through-thickness modulus with increasing volume content and axial stiffness of z-pins [55][58]. Experimental testing of z-pinned composite lap joints [56] has shown significant improvement to their ultimate strength and fatigue life [59]. z-Pinning does successfully improve all of the through thickness properties of the composite laminates but at the cost of significantly affecting the in-plane properties. The FEA [55][58] and experimental [60][61] evaluation of in-plane properties of laminates have suggested reductions to the either Young's modulus or shear modulus. Elastic properties have shown a

decreasing trend with the increase in z-pin diameter and volume % and this reduction depends on the amount of crimp and waviness in the fiber plies. Tensile [55][61] and compressive [57][62] strengths have also reported a reduction in z-Pinned laminates. Although fatigue life of lap joints have shown to increase by z-Pinning, fatigue life of laminates are affected under cyclic tension [61].

2.3.4. Stitching

Stitching involves sewing of high tensile strength yarns like glass, carbon and Kevlar through dry fabric plies and in rare cases uncured prepregs. Stitching density used is around 3-10 stitches/cm^2 [63].Stitching has been done since early 80s in manufacturing advanced 3D composite materials to provide through thickness reinforcements to FRP joints. Since then stitching has been done successfully on 2D laminates to achieve improved high energy impact damage tolerance [64], better delamination resistance, higher modes I and II interlaminar fracture toughness and for modest improvement in through thickness tensile modulus and strength [65][66][67]. It has been reported that the strength of stitched joints significantly improved in comparison to composite joints [68]. Improved delamination resistance provided by stitching is due to the bridging action of the stitches, which exert a closure traction force that lowers the tensile strain acting on the crack tip [69]. Stitching also slows down crack growth rate by reducing the tensile stress acting on tip [70]. Researchers have also noted that stitched joints are more prone to accelerated environmental degradation. Stitching does affect the in-plane mechanical properties like tension, compression and flexure

up to some extent [65][71]. Stitching also reduces the compression fatigue life and tension tension fatigue resistance of composites [69]

2.3.5. 3D Braiding

3D braided fiber architecture can be manufactured using varied techniques. Resultant composite properties depends heavily on the yarn size, angle of the braiding yarns, percentage content of axial yarns in the braid and the interlinked nature of 3D braid. It was reported that the tensile and compressive properties of the composite were increased when the braiding yarn angle was reduced but at the cost of transverse properties. 8 degree reduction in the braid angle improved about 25-50% of the longitudinal properties [72]. The 3D braided architecture imparts improved fracture toughness and better damage characteristics to the composites. Mode I interlaminar farcture toughness of braided composites is reported to be 2-4 times higher than traditional composites [73]. 3D braids were also reported to retain 86-99% of their gross tensile strength under open hole tension test as compared to 49% retained by 2D laminate. Due to the presence of certain amount of crimping in the yarns, the in-plane properties of 3D braided composites can never match that of 2D laminates. The most important limiting factor in 3D braided composites is the mechanical property loss observed when the braid edge is cut. 66% reduction in tensile strength and 40% reduction in tensile modulus were observed [74]; hence any machining of the braided surface which will result in braiding yarn becoming non-continuous will result in lower performance [69].

2.3.6. 3D Woven Composites

3D woven composite is a new type of advanced engineering material that is currently used in only a few niche applications. It has an added yarn in the z-direction called as z-binder. 3D woven composites have a very high resistance to delamination cracking in comparison to 2D laminates. Most of the delamination research has been focused on mode I loading of 3D woven composites while less has been done on mode II delamination properties. Delamination toughness of 3D carbon/epoxy with 1% z-binder was reported to be 14 times higher than a 2D carbon/epoxy prepreg laminate [75] and that of a 3D woven composite with 8 volume % of z-binder was reported to be 20 times higher than a 2D laminate [76]. Significant improvement in the delamination toughness of 3D woven composites was attributed to the toughening process of debonding, bridging, z-binders pull-out and crack branching. Work done on Mode II loading of 3D woven composite suggested a 2-3 times increase in the G_{IIC} over a 2D carbon-epoxy prepreg laminate [77]. As reported in braiding and z-pinning, even 3D woven composite's in-plane properties are lower than that of 2D laminates owing to the crimp and waviness of the load bearing fibers caused by z-binders in interlock 3D fabrics and resin pockets in orthogonal woven 3D fabrics. 35% lower Young's modulus has been reported for a 3D woven composite in comparison to 2D laminates [69]. Other reports have shown the reduction to be in the range of 10-35% [78]. A decrease of 20% and 30% was reported in the flexural modulus and strength respectively of a 3D woven composite as compared to 2D laminates [79].

2.3.7. Effect of Weave structure of 2D woven fabric on Inter-laminar fracture behavior

Hamada et al. (1996) [80] studied the effect of weave structure on Mode I inter-laminar fracture toughness by varying the weave structure at the midplane of laminate. Utilizing the fact that front and back structure of satin woven fabric is different, they fabricated three different laminates, 1) upper and bottom plies were put together symmetrically with their back structures facing each other in mid-plane (A), 2) upper and bottom plies are put together asymmetrically with their back structure facing the front in mid plane (B) and 3) upper and bottom plies put together in reverse symmetry with their front structures facing in the mid-plane (C). Higher fracture toughness of Specimen C compared to A and B was attributed to higher number of transverse fiber strands obstructing the crack path which act as the tougher region in the crack propagating plane.

Along with the weave patterns, Wang et al. (1994) [81] also studied the effect of adding low weight fractions of microfibers to epoxy matrix on the interlaminar fracture toughness. Fiberglass fabrics with triple plain and plain weave and Kevlar fabrics of plain weave and 5H satin weave were used and three types of microfibers were used. G_{Ic} values were reported to increase with increase in the number of fabric layers owing to the presence of lesser resin rich areas and hence reduction in the low resistance path for interlaminar crack. Composite samples with microfibers reported a 75-108% increase in fracture energy. The increase was attributed to microfibers enhancing the mechanical properties of resin rich

areas by rupturing, fibrillating and pull out mechanisms in the plane of crack propagation which increased the toughness.

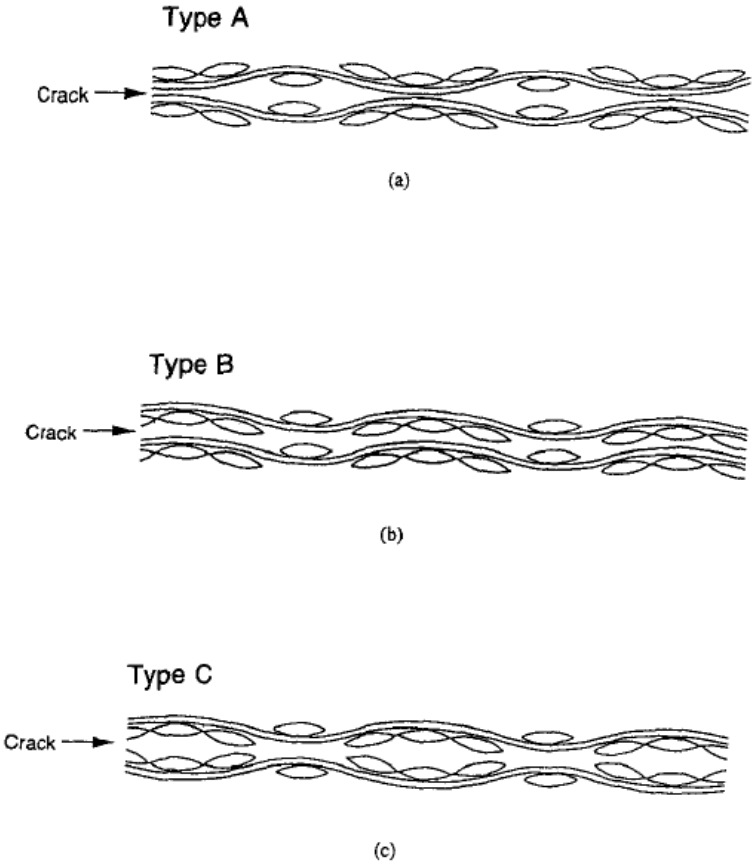

Figure 2-6: Mid-plane ply arrangement-(a) Symmetric-backs structure facing each other; (b) front structure facing back structure; (c) Symmetric-front structure facing each other [80].

2.3.8. Interleaving:

Commercially introduced by American Cyanamid as HST-7, interleaved composites are seen as a composite within a composite [45][82]. A discrete layer of very

high toughness and shear strain is added to the standard prepreg. Interleaf co-cures with the matrix resin and its flow control keeps it as a discrete layer throughout the process. Interleaved materials have a better compression after impact property [82]. Selective toughening using interleaves is also possible.

Chen et al. (1991) [83] studied the effect of interleaving as a toughening mechanism for graphite/epoxy composites. They produced interleaves by mixing carboxyl terminated butadiene-acrylonitrile (CTBN) and polyurethane with epoxy resin and preheating to 60 deg C until homogenous mixture was formed. Then pre-heated curing agents were added and mixed to this mixture followed by degassing and spraying thin interleaves between every two adjacent prepreg plies. Mode I testing on different interleaved specimen showed 25-50% increase in G_{IC} however author believes that G_{Ic} value did not represent the true effect of interleaving because of the presence of fiber bridging phenomenon, whereas Mode II gave a better idea of interleaf reinforcing the composite as the interleaf resin appeared capable of undergoing extensive plastic deformation. 2-3 times better G_{IIc} values were achieved over baseline specimens using interleaves and the increase was attributed to the high energy dissipating capability under complex stress fields at interlaminar zone. Author also set a correlation. Higher the fracture toughness ($G_{Ic)}$ of the interleaf resin better is the interlaminar cracking resistance (G_{IIc}) of the corresponding interleaved laminates.

Aksoy et al. (1992) [84] studied the effect of an amorphous thermoplastic and a nitride rubber modified epoxy thermoset interleaves on the interlaminar shear fracture toughness of graphite/epoxy composite plies. Results showed that there was significant

increase in G_{IIc} for both types of interleaves but Thermoplastic interleaf was more effective than thermoset interleaf because of a favourable combination of high yield strength and strain to failure. Where shear yielding around the crack tip was main mechanism responsible for toughness enhancement, thermoplastic interleaf indicated very little micro-cracking whereas thermoset material failed by extensive micro-cracking at 45 degrees to the crack plane.

Khan et al. (2012) [85] studied the effect of interleaves made by vacuum infiltration of carbon nanofiber bucky papers by epoxy resin, on carbon fiber reinforced composites. Mechanical testing on the interleaved CFRP showed 31% increase in ILSS and 104% increase in the Mode II interlaminar fracture toughness as compared to the baseline CFRP. Flexural modulus and strength seemed to be lower than that of baseline specimens but the magnitude was not significant. Increase in G_{IIc} was attributed to the microscopic mechanisms like CNF pull out and bridging mechanisms as well as crack deflection and meandering as seen macroscopically.

2.4. Carbon Nanotube Modified Composite Laminates

Owing to its multi-functional low density structure with superior mechanical properties, CNTs are being seriously considered to be used as a polymer composite reinforcement. They are used as nano-scale fillers to toughen the brittle polymer matrix. It is also used in traditional composite laminates in various forms to improve their through thickness properties like interlaminar fracture toughness which helps improve delamination

resistance and achieve higher tolerance to impact damage. Here we will discuss the research done on the use of CNTs in polymer composites using various techniques:

2.4.1. Dispersing CNTs into Matrix Material

Gong et al. (2000) [86] investigated the role of non-ionic surfactant on thermo-mechanical properties of CNT/ polymer composites. 1% CNT's were added to the polyoxyethylene 8 lauryl and acetone mixture which was magnetically stirred to achieve proper dispersion. Epoxy and hardener were then added to this mixture and was further stirred to achieve a homogenous mixture. This was then poured into mold and was cured at room as well as elevated temperature to make the desired samples. Tests showed 30% increase in elastic modulus of the composite with CNT and surfactant as compared to baseline sample with the glass transition temperature increasing from 63 C to 88 C, whereas the addition of CNT's without surfactant did not show this improvement. This improvement was therefore attributed to the presence of surfactant which made possible better dispersion of CNT in the matrix. Similar experiments were done on other nanoparticles.

Kim et al. (2008) [87] demonstrated the effect on fracture toughness of epoxy matrix modified with nanoparticles like carbon black and nanoclay. The nanoparticles were mixed in modified bis-phenol-A type epoxy resin in three steps; room temperature hand mixing, magnetic stirring at 60 deg C followed by 5 repeat cycles of batchwise three roll milling. The suspension was then mixed with hardener and was cured at 125 deg C for 2h. Fracture toughness measurements showed 23% increase in K_{Ic} on addition of 3 wt% Carbon black

whereas 20% and 50% rise in K_{IC} was witnessed on addition of 0.5 wt% and 3.0 wt% of nanoclay respectively. This shows that if proper dispersion is achieved, 1 wt% of CNT can be as effective as 3 wt% of other nanoparticles used.

Karapappas et al. (2009) [88] studied the change in fracture energy of CFRPs caused by reinforcing different amount of multiwalled CNTs. Dispersion of 0.1%, 0.5% and 1% of CNTs in epoxy matrix was done using high shear forces caused by high speed rotating disk of a torus mill device. Sixteen plies of uni-directional (UD) Carbon fibers were then hand laid-up followed by curing in an autoclave using vacuum bag technique. Mode I testing showed significant increase in fracture energy (60%) for 1.0 wt% of CNTs. Mode II testing too showed 45% and 75% increase for 0.5 wt% and 1.0 wt% CNTs respectively owing to fiber bridging and fiber pull-out. Both modes showed a decrease in fracture energy for 0.1 wt% of CNT which was attributed to the presence of agglomeration of CNTs in the final composite.

Mathivanan et al (2012) worked on improving the delamination resistance and tensile strength of woven GFRP using graphite powder (3%) modified epoxy matrix. A novel agitation technique was used to disperse graphite powder into the matrix. E-glass plain weave roving fabric was then hand lay up using modified matrix ply by ply followed by consolidation. Tensile test results on Modified GFRP showed 11% increase in the property over baseline specimen where as G_{IIc} values were not affected significantly. Instead the G_{IIc} value for modified GFRP gave a value less than that of baseline specimen.

Warrier et al. (2010) [90] studied the effect of dispersing 0.5 wt% CNTs directly in to fiber sizing or in to the Matrix on Glass/epoxy composites. Mode I fracture toughness testing results showed 10% and 25% increase in G_{Ic} at initiation owing to crack bridging and fiber pullout but G_{Ic} propagation value showed a 53% and 51% decrease for CNTs in sizing and CNTs in matrix respectively as compared to baseline. Adding CNTs to both sizing and matrix showed 28% increase in GIc initiation and a 34% decrease in GIc propagation. This decrease was attributed to the jeopardized bridging due to bundling of fibers in CNT sized glass fibers making the bundles more rigid making fiber bridging more difficult.

Godara et al. (2009) [91] produced prepregs using carbon fiber and different types of CNTs dispersed epoxy matrix. They used 0.5 wt% of MWCNT, thin MWCNT, amine functionalized DWCNT and compatilbilizer modified MWCNT. The prepregs were then cut and 8 plies were laid up to make laminates using vacuum bags and high temperature curing. Mechanical tests showed that there was a reduction in longitudinal tensile strength of up to 20% which was attributed to CNTs acting as defects and increasing stress build up around broken fibers. Mode I tests showed 75% increase in GIc for crack initiation and 83% increase in GIc for crack propagation for Modified MWCNTs being the highest of all. This increase was attributed to optimal dispersion, (increased affinity between CNTs and matrix) interfacial interaction of CNTs with matrix and its adequate toughening by crack bridging and crack deflection.

2.4.2. Spraying, Transfer Printing and Electrophoresis

Joshi et al. (2011) [92] demonstrated a novel technique of dispersing CNTs on prepregs, and hence enhancing interlaminar fracture properties. A 14 ply plain weaved carbon fiber prepreg laminated was made where CNTs were dispersed at the midplane. Laminate was then cured under vacuum with added pressure at 120 deg C which could have caused the interlocking of CNTs with layers next to mid-plane plies. Fracture toughness testing of a specimen containing 1.32g/cm^2 CNTs at midplane showed 40% and 32% rise in the value of G_{Ic} at initiation and propagation respectively. The rise in Mode II fracture toughness was 140% which was attributed to significant fiber bridging and strong fiber matrix adhesion.

Garcia et al. (2008) [93] transfer printed the vertically aligned CNTs at the midplane interface between plies of carbon prepreg and laminates were consolidated using vacuum and cured in an autoclave. Mode I and Mode II test results showed enhanced toughness which was attributed to nano-stitching, fiber pull out and nanotubes bridging the two plies. 3X increase in G_{IIc} values was considered significant as compared to 1X increase achieved in standard stitching and z-fiber reinforcement. G_{Ic} showed 2.5X increase as compared to baseline specimen. While promising, the CNT array transfer method is severely hampered by the small size of grown CNT arrays as compared to the size of laminated composites.

Woven carbon fabric was selectively coated with single and multiwalled carbon nanotubes using Electrophoresis [94]. Electrophoretic dispersion of CNT on positive electrode was based on their ability to respond to electric field. Assembly of carbon fabric as

positive electrode and steel plate as counter electrode was placed in a CNT dispersed water bath. CNTs being electrically conductive responded to the applied potential of 10V/cm and deposited uniformly. The CNT-Carbon fabric preform was then consolidated using VARTM process with epoxy matrix. 30% increase in Interlaminar strength was reported for the CNT-Carbon fabric-epoxy composite compared to the carbon fabric-epoxy composite.

2.4.3. Growing CNTs directly on Fiber Tows

Wicks et al. (2009) [95] explored the effects reinforcing aligned Carbon nanotubes in three dimensions. They grew 20-30 μm long radially aligned CNT's directly on the surface of alumina fiber woven cloth by modified thermal chemical vapor deposition using iron nitrate catalyst. They then hand layup the plies with room temperature degassed epoxy and consolidate the laminate under vacuum. This composite setup enhances the inter-laminar toughness in steady state by 76% (approx. 1.5kJ/m^2) and in initiation by 63%. Enhancement in the intra-laminar strength was also noted where the tension bearing response increased by 19%, 9% and 5% in bearing stiffness, critical strength and ultimate strength respectively. These enhancements in mechanical properties were attributed to the presence of aligned CNTs which acted as 3-d reinforcement for improving inter-laminar toughness and in plane reinforcement to improve intra-laminar strength. Similar work was done by Veedu et. al. [12] They grew well aligned multi walled CNTs, using CVD process, perpendicular to 2D woven SiC fabrics to produce 3D fabrics. CNT forests provided multifunctional properties along the thickness direction resulting in 3D effect between plies under loading. A significant rise of

348% over base composite was reported in the Mode I fracture toughness of the multifunctional composite and 54% rise was reported for Mode II fracture toughness.

Chapter 3 Testing of Composite Mechanical Properties

3.1. Mode I Interlaminar Fracture Toughness Testing

Double Cantilever Beam (DCB) test is used to measure Mode I interlaminar fracture toughness of composites. American standard ASTM D5528-01 (2007) [96], Japanese Industrial Standard JIS K 7086 (1993) [97] and ISO 15024 (2002) are the three standards currently in use for DCB testing. ASTM 5528-01 is used in this investigation. This test standard is limited to use with composites consisting of unidirectional carbon fiber and glass fiber tape laminates with brittle and tough single phase polymer matrices but it has been used extensively in literature for 2D woven textile composites [80][89][95] hence we will be using this method to test the interlaminar fracture toughness of 8 harness satin weave epoxy prepreg laminates. According to this method, specimens shall be atleast 125 mm long and 20-25 mm wide. The insert length should approximately be 63mm which constitutes of 50 mm of initial delamination and the rest used to bond loading fixtures (hinges or load blocks). Loading fixtures should be as wide as the specimen. Stainless steel piano hinges have been used in this investigation for applying Mode I loading to the specimens. The laminate thickness should normally be between 3-5 mm with a 0.1 mm tolerance.

Interpretation of Test Results

Initiations G_{Ic} values are determined using 3 different techniques stated as Deviation from Linearity (NL), Visual Observation (VIS) and 5% offset maximum load.

NL G_{Ic} point is typically the lowest of all. It is calculated from the load and displacement data where the graph deviates from linearity i.e from the onset of Nonlinearity (NL). It is assumed that delamination grows in the inside of the specimen. It is specially the case with tough matrix composites where a region of nonlinear behavior may precede.

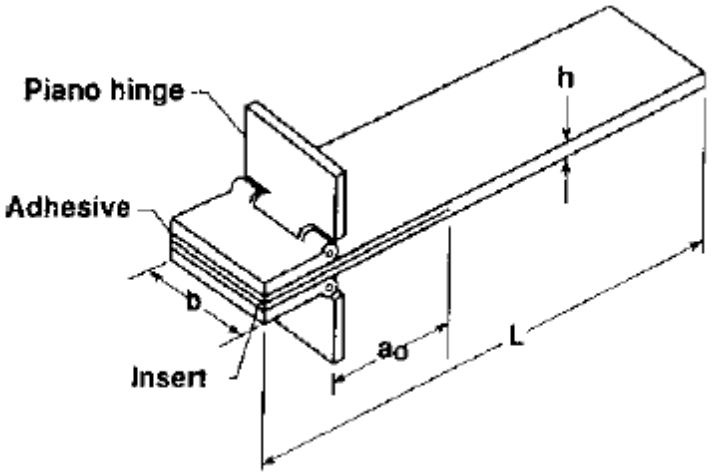

Figure 3-1: DCB Specimen [96]

Visual Observation of crack front is done to determine the delamination onset at the specimen edges. A visual observation point is where the delamination is visible and is measured on any one edge of the specimen.

5% offset point is the intersection of the load vs displacement curve and the line drawn from origin and offset by 5 % increase in compliance from the initial linear region of the curve. If

the intersection occurs after the maximum load point, maximum load should be used to calculate G_{Ic}.

G_{Ic} Calculation

There data reduction methods are provided in the ASTM standard for calculating G_{Ic}, namely modified beam theory (MBT), compliance calibration (CC) and modified compliance calibration (MCC).

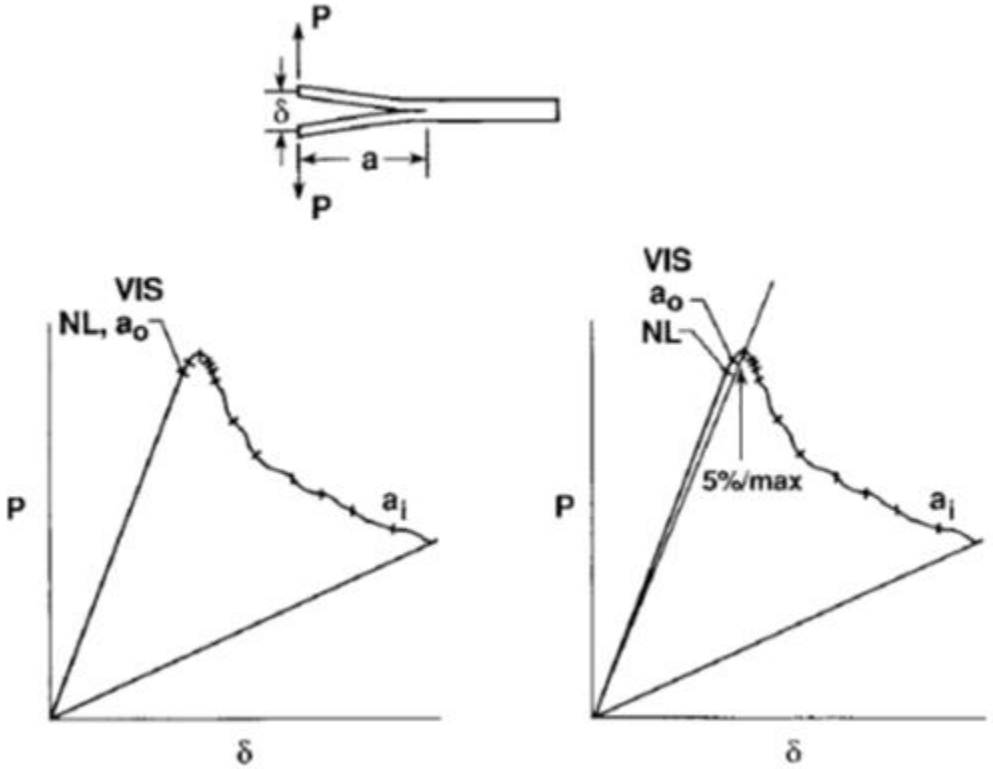

Figure 3-2: NL, VIS and 5% values on the Load vs Displacement curve for brittle and tough matrix [96]

Modified beam theory data reduction method is recommended by ASTM D 5528-01 since it yielded most conservative values of G_{Ic} for 80% of their tested specimens. It accounts for the rotation at the delamination front since the beam is not perfectly built in; hence it is assumed that the specimen contains a slightly longer delamination (Δ) then a_0 and the crack length used is $a_0+|\Delta|$, where Δ is found by fitting the line of least squares on the '$C^{1/3}$ vs a' curve where C is the ratio of the load point displacement to the applied load.

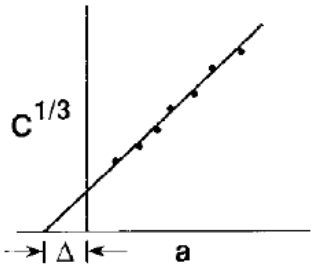

Figure 3-3: Cube-root of compliance vs crack growth curve [96]

3.2. Mode II Interlaminar Fracture Toughness Testing

End Notched Flexure (ENF) test is used to measure Mode II interlaminar fracture toughness. Japanese Industrial Standard JIS K 7086 (1993) [97] is currently in use for ENF testing. ENF test is used to determine only the initial stage mode II interlaminar fracture toughness. Due to the unstable crack propagation achieved during testing, it is not possible to achieve the propagation values for G_{IIc} using this test method. 3 point bending machine is used to apply the forward shear mode II loading to the specimen. The following figure and table shows the ENF test requirements for the machine and specimen.

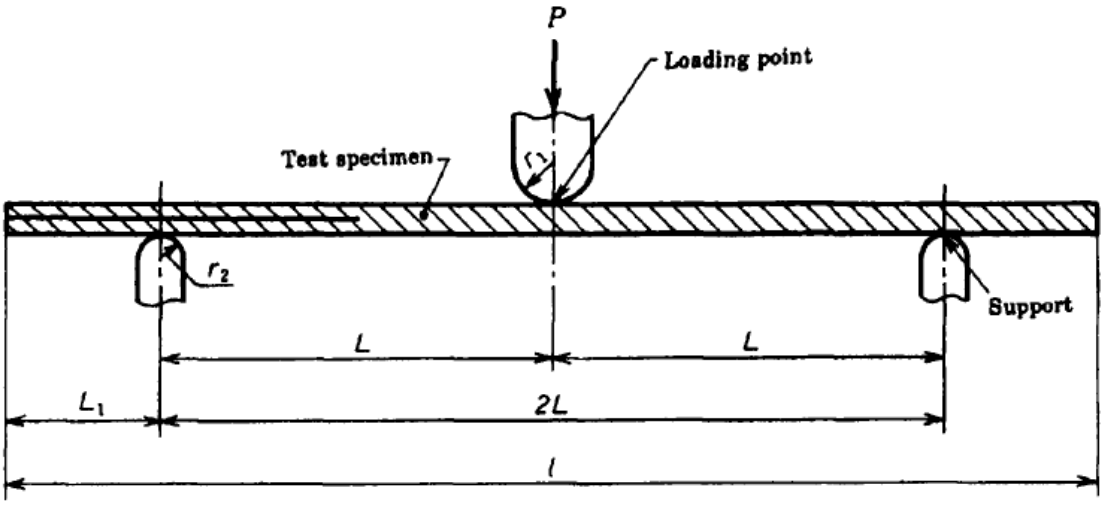

Figure 3-4: Testing Apparatus for ENF test [97]

Table 3-1: ENF Specimen Dimensions as specified in JIS K 7086 (1993) [97]

Mark	Section	Dimension (mm)
L	Distance from support to loading point	50 ± 0.2
L_1	Overhang	20 – 25
L	Length of test specimen	140 – 150
r_1	Radius of loading nose	5 ± 0.1
r_2	Radius of support	2 ± 0.2

Interpretation of test result

Classical plate theory method described in JIS K 7086 is used to calculate G_{IIc} value in the ENF method. Compliance and Critical load values are needed to proceed with this method. Inverse of the slope of the load vs load line displacement curve is used to calculate compliance, whereas to calculate critical load; a straight line is drawn from origin and offset by 5% increase in compliance from the initial linear region of the curve. If the intersection of the offset line and the curve occurred before the maximum load, then the

intersection value of the curve was used as the critical load, else maximum load was used as the critical load.

3.3. Tensile Properties of Polymer Matrix Composite Materials

ASTM D3039/D3039M-08 is used to test the tensile properties of the composite specimen. Here a thin flat strip of a material with a constant rectangular cross-section is mounted in the grips of tensile tester and is loaded in tension. This method determines the in-plane properties of polymer matrix composite materials reinforced by high modulus fibers [98]. The stress-strain response of the material can be determined by measuring the strain using displacement transducers. This method requires the laminates to be balanced and symmetric. Tensile property data is generated for various applications like research and development, quality assurance, structural design and analysis. Care must be taken to eliminate any bending produced in the specimen from the test fixtures as it may cause pre-mature failure and under-estimate the strength and modulus.

The tensile specimen and geometry specifications required are listed in tables 3-2 and table 3-3.

Interpretation of Results

Stress values are to be calculated for each data point from the available Load data and specimen dimensions. Ultimate tensile strength is calculated using the maximum load data point and is supposed to be reported up to 3 significant figures. Tensile chord modulus of elasticity is calculated and reported up to three significant figures.

Table 3-2: Tensile Specimen General Geometry Requirements as specified in ASTM D 3039 [98]

Parameter	Requirement
Coupon Requirements:	
Shape	Constant rectangular cross-section
Minimum length	Gripping + 2 times width + gage length
Specimen width	As needed
Specimen width tolerance	± 1% of width
Specimen thickness	As needed
Specimen thickness tolerance	± 4% of thickness
Tab Requirements:	
Tab bevel angle	$5 – 90^{o}$, inclusive
Tab step at bevel to specimen	Feathered without damaging specimen

Table 3-3: Tensile Specimen Specific Geometry Requirements as specified in ASTM D 3039 [98]

Fiber Orientation	Width (mm)	Length (mm)	Thickness (mm)	Tab Length (mm)	Tab bevel angle, ^{o}
0^{o} unidirectional	15	250	1.0	56	7 or 90
90^{o} unidirectional	25	175	2.0	25	90
Balanced and symmetric	25	250	2.5	Emery cloth	-
Random-discontinuous	25	250	2.5	Emery cloth	-

3.4. Short-Beam Strength of Polymer Matrix Composite Materials

ASTM D 2344/D 2344M-00 is used to measure short beam strength of high-modulus fiber-reinforced composite materials [99].A short beam with thickness up to 6.00 mm is machined from laminated composite and is centre-loaded to be tested in a 3-point bending fixture. This method was used initially to determine short beam shear strength of composite materials but later in 2000 it was revised and the word shear was removed from its title owing to the complex internal stresses generated during the test leading to various failure modes. The failures that occur during 3-point bending in short beam strength are majorly

matrix related shear failures accompanied by crushing or bending failures which depends on the span length to thickness ratio used. A minimum specimen thickness used is 2.0 mm and this test is limited to use the loading span length-to-specimen thickness ratio of 4.0. Suggested specimen length to thickness ratio is 6.0 and specimen width to thickness ratio is 2.0.

Maximum load observed during the test is noted using load-load point displacement data and is used along with specimen dimensions to calculate the short beam strength.

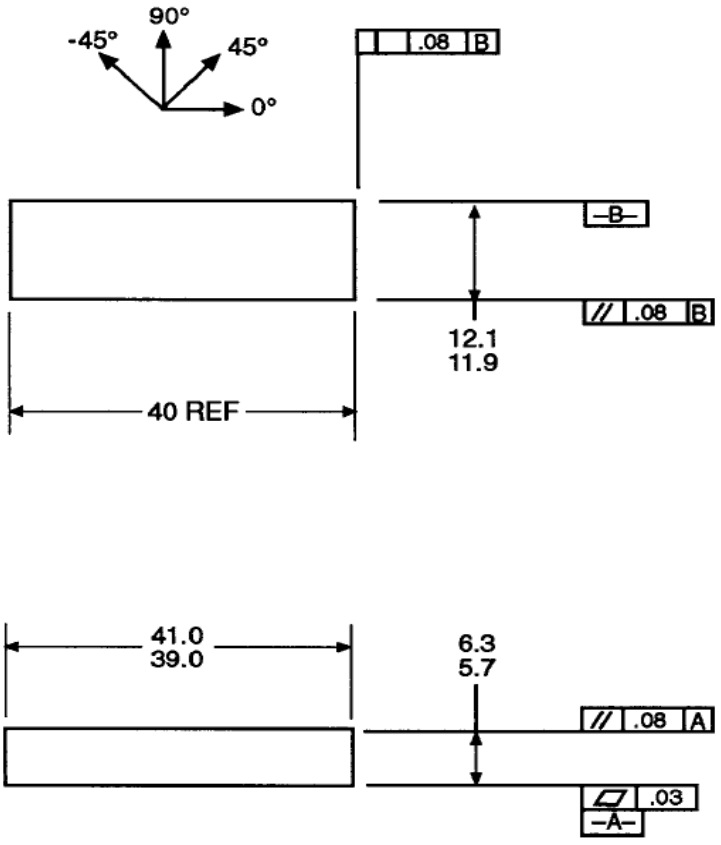

Figure 3-5: Short Beam Strength Specimen Dimensions as required by ASTM D 2344 [99]

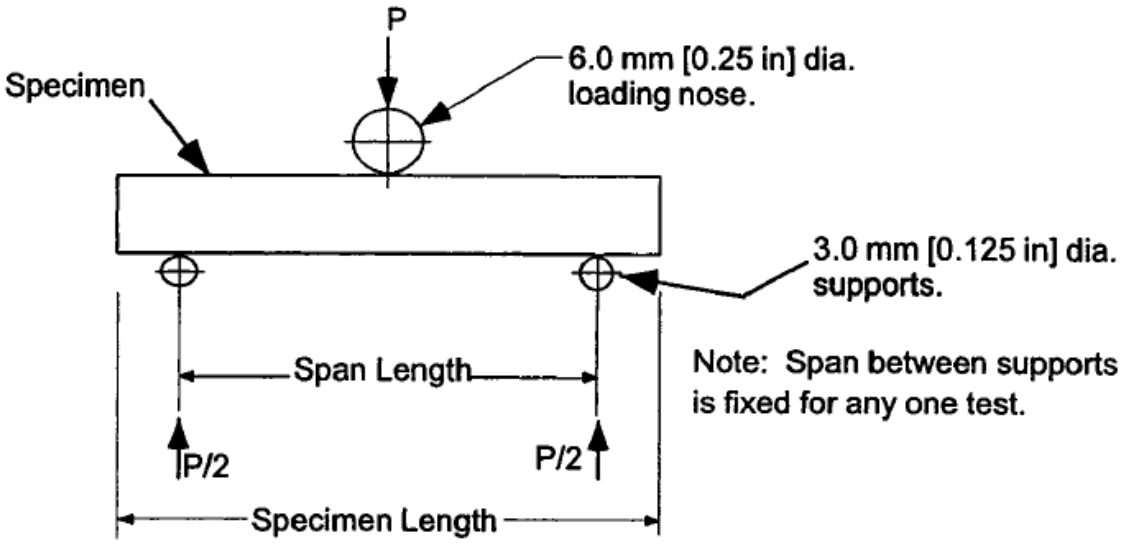

Figure 3-6: Loading and Support Nose Dimensions specified in ASTM D 2344 [99]

Chapter 4 Experimental Section

Glass fiber reinforced epoxy matrix prepregs were used as a raw material to make composite laminates. Carbon nanotubes used to modify these laminates were self synthesized in Dr. Bradford's laboratory using low pressure chemical vapor deposition technique.

4.1. Drawable CNT array synthesis

Low pressure chemical vapor deposition system was used to grow drawable CNT arrays on a quartz substrate using vapor phase Iron chloride as a catalyst. Acetylene gas was used as a precursor and chlorine gas was used for a post-treatment.

A 76 mm diameter quartz tube was used as a furnace chamber; also called as outer tube. Inner tube of 64 mm diameter and 74 cm length was inserted inside the outer tube and was used to load the 3 in. by 1 in. quartz substrates for CNT growth. Substrates and both the tubes are burnt at 800^{o} C for 10 minutes to burn off carbon based impurities on their surface. Then the inner tube and the substrate are etched in a hydrofluoric acid bath for 1.5 hr. This treatment is done to achieve a pristine quartz outer layer without any impurities. This was followed by rinsing with de-ionized water. Substrates were then dried using a high pressure nitrogen gun whereas the inner tube is cleaned using non-woven wipers and ethanol. The substrate was then placed on a quartz stage inside the inner tube. 1gm iron chloride catalyst, which is stored inside an air tight dessicator, was weighed using a digital balance and placed in a quartz boat partly under the quartz stage inside inner tube.

Figure 4-1: Low Pressure Chemical Vapor Deposition System

The quartz stage is kept in the middle of the tube where the temperature range seems to be constant. The whole system is then closed and pumped down for 2-3 hours to achieve the inner tube pressure to be around 7-8 mTorr using vacuum pump before starting the growth run. This is done to remove the air and water vapor impurities from the tube. Once the system is pumped down, the growth run is carried out under following growth conditions:

Temperature: 760^{o} C, Pressure: 3 Torr, Growth Time: 15 minutes, Gas constituents: Acetylene – 600 sccm, Chlorine – 0.133 sccm and Argon – 0.267 sccm.

This treatment is followed by 20 minute chlorine post-treatment to achieve drawable CNT array, where the temperature and pressure remains the same but acetylene and argon gas flows are stopped by turning their individual mass flow controller off.

Iron chloride is vaporized completely around 550^{o} C. It coats every quartz surface it comes in contact with. The gases are released in to the system using their mass flow controllers, once the temperature reaches 760^{o} C and the pressure is controlled by an automatic pressure control valve. The reaction dynamics inside the furnace during growth is based on the chloride mediated chemical vapor deposition method as explained above. Carbon nanotubes arrays grown using this procedure were 1.4 mm to 1.5 mm tall and could be successfully drawn into sheets.

Drawing CNT Sheets: CNT arrays grown using above specified conditions were found to be easily drawable. CNT ropes were drawn from the array using tweezers. Multiple ropes were drawn out from one edge of the array and joined, such that the whole 1 inch wide sheet could be drawn.

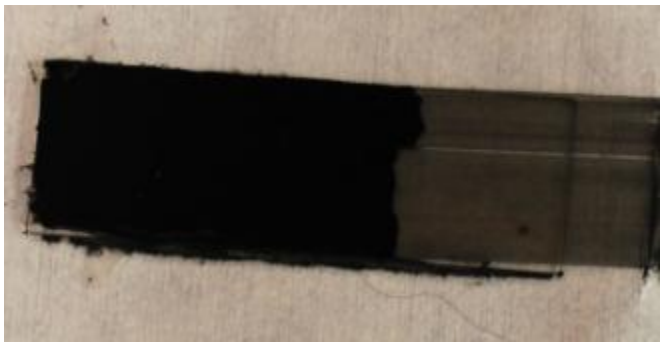

Figure 4-2: 1 inch wide CNT sheet drawn out of a 3inch by 1inch VACNT Array grown on a glass substrate

CNT-Sheet Characterization

Drawable CNTs used in this investigation were synthesized using low pressure chemical vapor deposition as explained above. Physical characterization of the as grown drawable CNT array and drawn CNT sheet is reported here.

A (3 in.×1in.) 76.2 mm×25.4 mm quartz substrate used for growing CNTs was covered fully by the as grown CNT array. Two such arrays were used for physical characterization. Array height of both the CNT array samples grown for 15minutes followed by a 20 minute post treatment measured using an optical microscope was found to be 1.4 mm. CNT sheets from both the samples were drawn on to a motor driven aluminum tube with a circumference (6.00 in.) 152.4 mm at the rate of 25 revolutions per minute. The length and width of the CNT sheet drawn from (3 in. ×1in.) 76.2 mm×25.4 mm substrate measured using digital calipers was found to be (5.972 in.) 151.68 mm and (0.95 in.) 24.13 mm respectively. Area of the as-drawn CNT sheet per revolution was calculated to be 3.661×10^{-3} m^2. CNT sheet drawn from Array-1 was wound for 168 revolutions (Sample-1) and that from Array-2 was wound for 120 revolutions (Sample-2). 120 layer of as-drawn CNT sheet was measured to be 2.65 mm thick. Successful measurement for 168 layered CNT sheet was not possible because the sample was too thick to be cut from the tube and straightened without major folds in the structure. Sample-1 weighed 0.1103 g and Sample-2 weighed 0.057g. 51.5 mm and 40.32 mm of array length was used from sample 1 and sample 2 for winding 168 and 120 revolutions respectively. Values for physical characterization are listed in Table 4.1.

Table 4-1: CNT aligned sheet characterization results

Property	Sample 1	Sample 2
Areal Density-CNT sheet (g/m^2)	0.1772	0.1388
Area covered by CNT sheet wound from 3"x1" CNT array (m^2)	0.91	0.831
Volumetric Density-CNT array (g/cm^3)	0.07886	-
Volumetric Density- CNT sheet (g/cm^3)	-	0.00628
Area of CNT Sheets per unit weight of CNTs (m^2/g)	5.64	7.204

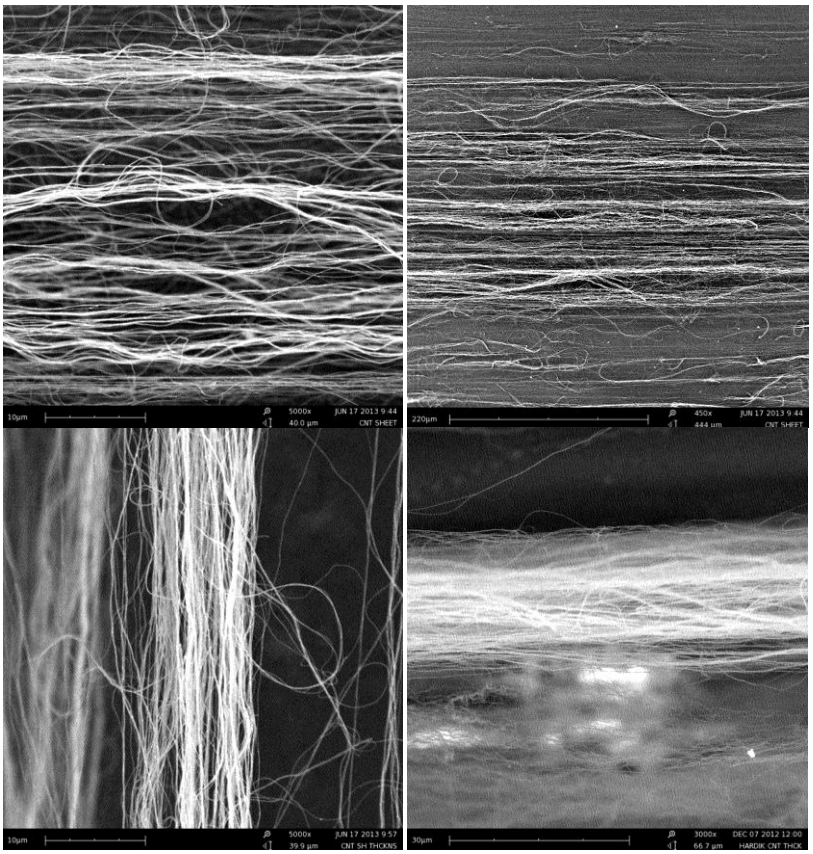

Figure 4-3: SEM images of the aligned CNT sheet: top view (top two images) and side view (bottom two images)

4.2. Laminate Fabrication

8 Harness Satin Weave 7781 E-Glass fabrics pre-impregnated with an epoxy resin system were obtained from Fibre Glast Developments Corporation. Resin content of the

prepreg system ranged from 27.0% - 33.0%. Pre-preg system was used to achieve near-perfect resin content in to have the most repeatable strength properties for every laminated composite sample fabricated. The obtained prepreg fabric was covered on both the sides by plastic sheets to save it from airborne particles and other impurities which might damage the prepreg during storage.

The obtained prepreg fabric was cut into required dimensions using an automatic GERBER cutting machine to reduce the irregularities which arise in the hand cutting samples. Stacking of the cut prepreg plies was done using one of the symmetric variants used by Hamada et al., who studied the effect of weave structure at the mid-plane. This was necessary owing to different front and back structure of satin woven fabrics. Figure 2.7 shows 3 different mid-plane ply arrangements. Arrangement C was used throughout this investigation for stacking a symmetric sequence to fabricate the laminates. Laminates were made by stacking individual plies and appropriate pressure was applied to compact two plies using a hand roller.

Carbon nanotube modified laminate: Individual plies were modified using aligned CNT sheets. CNT sheets were drawn from the array and were laid on the prepreg ply. Owing to the ply's tackiness, the sheet easily stuck to the ply. The whole ply was covered using aligned CNT sheet. Two ways of aligning CNT sheets on the prepreg were used. The first way being parallel to the warp direction and the crack growth direction (0^o) whereas the second way being perpendicular to the warp direction and the crack growth direction (90^o).

The number of layers of CNT sheets used to cover the plies was varied depending upon the mechanical test and samples fabricated.

Prepreg ply layup was consolidated and cured by using vacuum and high pressure hot press. Steel plate was used as a one-sided base mould tool to achieve flat specimens and a vacuum bag is used as the counter mold. Teflon film is placed on the steel plate instead of a release agent which facilitates easy removal of laminate from the plate. Prepreg ply layup is placed between two nylon peel-ply sheets on the Teflon film. Peel ply is used here to facilitate the excess resin and air flow through it and also to provide textured surface used for secondary bonding to the laminate. High fill nonwoven polyester fabric was used as a bleeder cloth. Resin bleeder is used on the top of the peel-ply to soak up the excess resin and to evacuate the air and other gases produced during curing. It also facilitates even pressure throughout the laminate. Teflon film, peel ply and the bleeder cloth were hold in place on the steel plate using high temperature adhesive tape. The whole assembly is covered by using a nylon vacuum bag which can withstand temperature up to 400^{o} F. Vacuum bagging is sealed on the steel plate with one end of the pipe inside the assembly using the sealant tape. Platinum vacuum pump from JB industries was used to apply vacuum. Ultrasonic Leak Detector was used to identify the leaks if any and their intensities in the vacuum bagging. Vacuum is applied to the hand pressed CNT modified ply layup for debulking it. The whole assembly is then placed in a 50 Ton Wabash Hot Press. The load applied to the samples via the hot press was calculated by multiplying the composite area by the desired consolidation pressure.

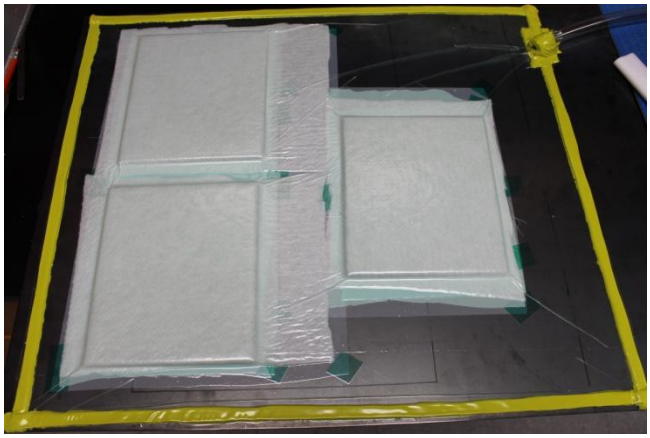

Figure 4-4: Stacked Laminate Consolidated using Vacuum

Figure 4-5: Curing the Consolidated Sample in 50 Ton Hot Press

The prepreg supplier recommended 3 curing cycles for its E-Glass prepregs which produces same end properties. All curing cycles had to start with a temperature ramp up from

room temperature to target temperature, hold the target temperature for a specific period of time and end with a ramp down to room temperature. Maximum ramp up and ramp down rate was suggested to be 5^{o} F per minute. Table 4.2 shows the three recommended cure cycles. The target temperature of 310^{o} F was used in this investigation to cure the composites with a hold time of 1 hour.

Table 4-2: Recommended Cure Cycles for Woven Glass Fiber Reinforced Epoxy Prepreg System

Cure Cycles	
Target Temperature	Hold Time
310^{o} F	1 hour
290^{o} F	2 hours
270^{o} F	4 hours

Extra pressure is applied to the layup in the hot press while it is curing. The vacuum bagged assembly is pressurized up to 40 psi and the temperature is ramped up simultaneously. When the temperature reaches 210 ^{o} F the pressure is raised from 40 psi to 55 psi. Platen temperature was controlled automatically and has a digital meter which helps checking the temperature and maintaining it at required temperature. Once the temperature reaches 310 ^{o} F it is held there for 1 hour to allow the matrix to cure. Figure 4.4 and Figure 4.5 shows the vacuum assembly and the hot press used to cure the composite. Platen heat is switched off after the hold time for the curing cycle is up and the assembly is allowed to air cool. We have to let the assembly cool naturally at the maximum rate of 5 ^{o} F or below till the temperature reaches 150 ^{o} F. Later we can use water assisted cooling to cool the assembly up to room

temperature at a faster rate. Once cooled, the laminate is taken out of the assembly and is cut to specimen dimensions using a wet diamond saw. 6 to 8 specimens were made from each sample.

4.3. Manufacturing Specimens for Mechanical Testing

DCB and ENF specimens required a crack starter in the mid-plane to simulate a crack opening for the Mode I and Mode II fracture toughness tests. A 24 ply symmetric laminate was stacked and consolidated to achieve a laminate thickness on the order of 4 mm – 5 mm. After laying 12 plies, a 60 mm long, 13 µm thick Teflon film was placed carefully onto the prepreg covering its entire width. Care was taken to remove any folds and creases in the Teflon film to reduce the possibility of artificial resin pockets and voids formation and achieve a smooth ripple free surface with the Teflon edge being perpendicular to the warp direction of the woven prepreg. The other plies were then laid symmetrically onto the first half with Teflon on it. The laminate is then consolidated and cured as explained above. Tensile samples and SBS samples did not require any such crack starter. A 12 ply symmetric laminate and a 32 ply symmetric laminate was stacked and consolidated to make Tensile and SBS specimens respectively, to achieve a laminate thickness on the order of 2-3 mm and 5-6 mm respectively. Samples fabricated for electrical resistance testing were similar to tensile testing samples.

Five different types of samples were made and tested using DCB test: Control, 4 Layer Perpendicular (basis weight of CNT fabric of 0.708 g/m^2), 8 Layer Perpendicular (basis weight of CNT fabric of 1.41 g/m^2), 2 Layer Parallel (basis weight of CNT fabric of

0.354 g/m^2) and 2 Layer Perpendicular (basis weight of CNT fabric of 0.354 g/m^2) and Three different types of samples were made and tested for the ENF, Tensile and SBS tests: Control, 2 Layer Parallel and 2 Layer Perpendicular. For the DCB and ENF samples; only the mid-plane was CNT modified, whereas for tensile testing samples and electrical resistance testing samples; aligned CNT sheets were introduced in between all the plies. To ensure that the shear failure for SBS samples occur in the CNT modified plies, 7 ply and 11 ply interfaces including the mid-plane were modified symmetrically.

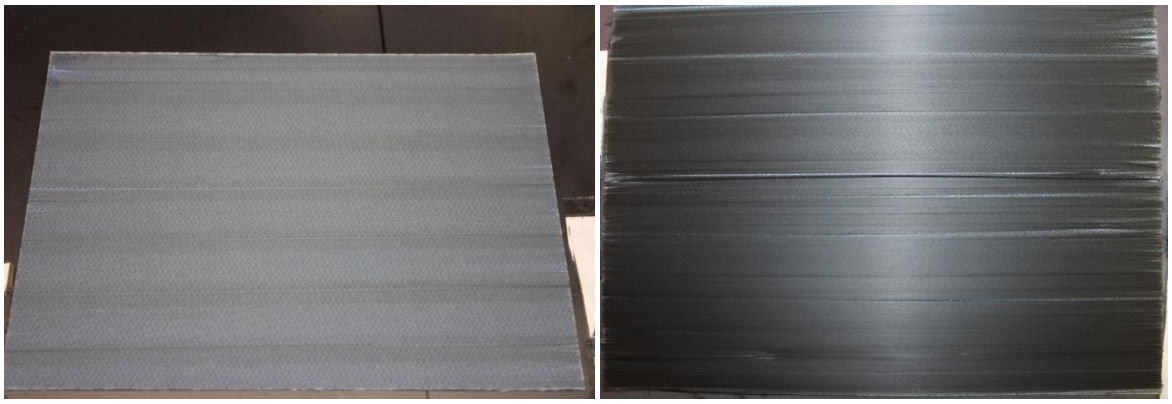

Figure 4-6: Single prepreg ply modified by aligned CNT sheet, a) 1 Layer aligned CNT sheet; b) 4 Layers of aligned CNT sheet

The number refers to the layers of aligned CNT sheets laid in the ply interface and the ‘Parallel’ and ‘Perpendicular’ refers to the direction of CNT sheet alignment with respect to the warp direction and the crack growth direction of the specimen.

A minimum of 5 specimens were tested to validate the results.

4.4. Test Methods:

4.4.1. Mode I IFT Test Procedure

ASTM D 5528-01 standard specifications were used to prepare DCB specimens. Piano hinges were used as loading fixtures and were glued to the composite specimen using epoxy paste adhesive from Henkel- Hysol EA 9309.3 NA with glass beads to achieve consistent bond-line thickness. White spray wass used to coat one side of the specimen so that the growing crack was more easily detected. Line markings were made on the coated side to determine the crack growth. Thin lines were marked at 1 mm intervals up to 5 mm and at 5 mm interval for the next 45 mm. The specimens with piano hinges were then mounted in the MTS Q-test tensile testing frame. Fig shows the DCB test setup. Hydraulically operated serrated grips were used to grip the hinges with a grip pressure of 1600 psi. A 1000 lb load cell was used to measure the load. A displacement controlled loading is applied to the specimen at the constant rate of 2 mm/min. Crack propagation was manually observed using a white light torch and a magnifying glass. Load and displacement values were noted manually for each marking when the crack propagated through it. The test was terminated after the crack propagated up to 50 mm. A full list of specimen dimensions is listed in Appendix 1.

The load vs load-displacement graphs were plotted for each tested specimen. Deviation from linearity (NL) was used to identify critical load and load point displacement values for calculating G_{Ic} Initiation. Modified beam theory method was used to calculate strain energy release rate for Mode I type fracture using the following equation [96].

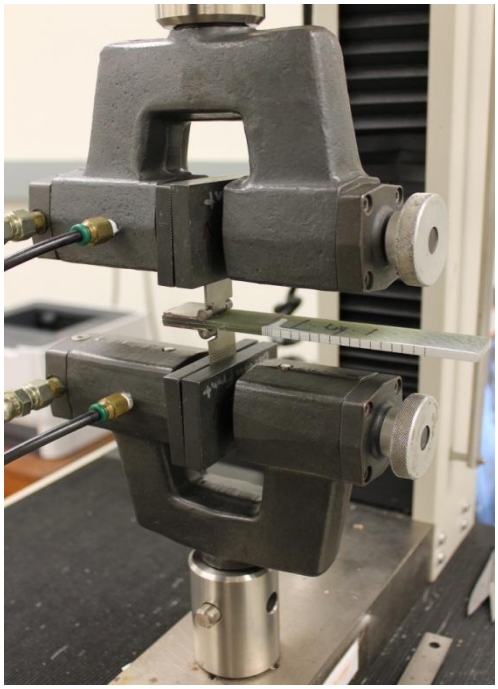

Figure 4-7: DCB test setup

$$GIc = \frac{3P\delta}{2b(a + |\Delta|)}$$

Where:
P = load,
δ = load point displacement,
b = specimen width,
a = delamination length,
C = compliance and,
Δ is calculated by fitting the line of least squares on the '$C^{1/3}$ vs a' curve.

4.4.2. Mode II IFT Test Procedure:

Specimens were loaded in 3-point bending test fixture where bending load is applied to obtain the forward-shear type fracture at the crack initiation at the point where the

crack starter ends. Specimens were supported throughout their width by the loading and support fixtures. Load was applied with a 3-point bending machine from Test Resources and was measured by a 1000 lb load cell. Figure 4.8 shows the test setup. Load point displacement was calculated using independent strain gage from Epsilon Technology Corporation. A displacement controlled loading was applied at the displacement rate of 0.501 mm/min. The test was programmed to be instantaneously terminated when the load fell to 50% of the maximum. Load vs load point displacement curves were plotted for each tested specimen. Compliance was calculated as the inverse of the slope of the line of least squares fitted at the initial elastic portion and at the initial critical load portion of the load vs load-displacement curves.

Strain energy release rate for Mode II type fracture at initiation is calculated using the following equation [97]:

$$a1 = [\frac{C1}{C0}a0^3 + \frac{2}{3}(\frac{C1}{C0} - 1)L^3]\text{^}(1/3)$$

$$G_{IIc} = \frac{9a1^2Pc^2C1^2}{2B(2L^3 + 3a1^3)}$$

Where,
G_{IIc}: initial stage interlaminar fracture toughness of mode II (kJ/m^2)
a_0: initial crack length (mm)
Pc: initial critical Load (N)
C_0: load point compliance at initial elastic portion (mm/N)
C_1: load point compliance for the initial critical load (mm/N)
a_1: calculated crack length for initial critical load (mm)
L: distance between supporting point and loading point (mm)
B: width of test specimen (mm)

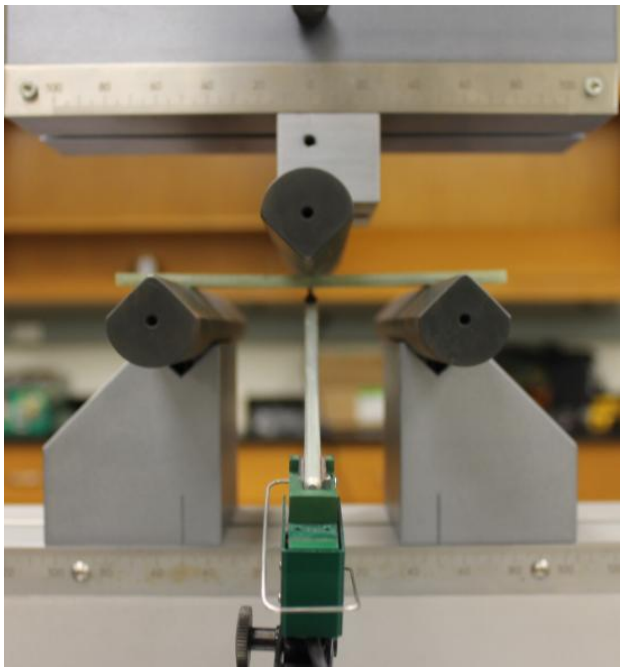

Figure 4-8: ENF Test Setup

ENF test requirements as specified in JIS K 7086 (1993) are shown in the previous section but we used slight modification of the parameters of machine and specimens. Although the radius of loading nose and support nose specified in the test are 5 mm and 2 mm respectively, we used 6 mm radius for all the three fixtures due to the availability of these fixtures. Specimen dimensions are listed in Appendix 1.

4.4.3. Procedure for Tensile Testing of Composite Specimens:

Specimens were cut keeping in mind the dimension guidelines given in the standard for 0^o laminates as well as 90^o laminates since the material used here was a woven fabric

which includes fibers in both the above mentioned directions. The length of the specimens used was 250 mm which correspond to 0^o direction whereas the width and thickness of the specimens were around 20 mm and 2.2 mm respectively which correspond to 90^o direction. A full list of each specimen dimensions is listed in the appendix. Glass fiber epoxy matrix

Table 4-3: ENF Specimen and Machine Dimensions used in this Investigation

Mark	Section	Dimension (mm)
L	Distance from support to loading point	50
L_1	Overhang	29
L	Length of test specimen	158
r_1	Radius of loading nose	6
r_2	Radius of support	6

laminates with a smooth surface finish were used as tabbing material. 56 mm of tab length was bonded using epoxy paste adhesive from Henkel- Hysol EA 9309.3 NA with glass beads to achieve consistent bond-line thickness. The tab taper angle used was 90^o since it was one of the suggested tab geometries common in both the 0^o laminates as well as 90^o laminates. The tabbed specimen was placed in the hydraulic grips of MTS tensile tester where its alignment was tested using a vertical laser marker. Care was taken to extend the grip jaws beyond the tabbed region by 5mm approximately to save the specimen from failing at the tab end. Laser extensometer was used to measure the sample strain. Two laser reflective strips were taped 20 mm apart on the sample and the extensometer was calibrated at that position to measure a ‘zero’ 0 reading. A displacement controlled test at the displacement rate of 1 mm/min was used to carry out tensile testing.

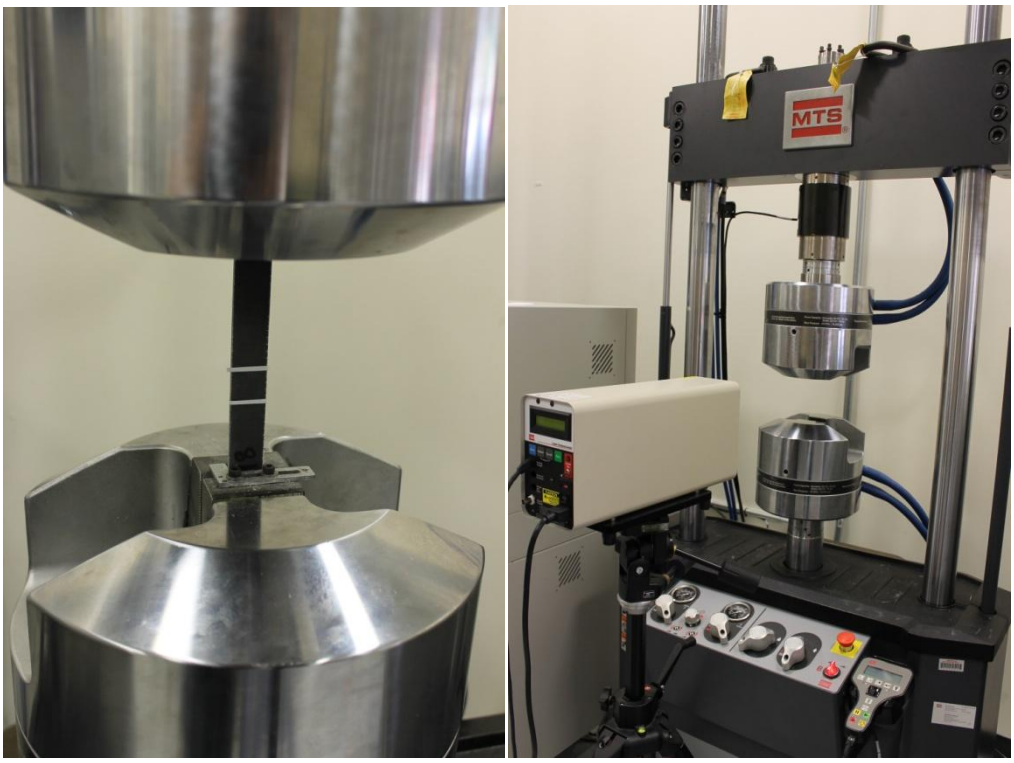

Figure 4-9: Tensile Test Setup

Ultimate Tensile Strength was calculated using the following equation:

$F^{tu} = P_{max}/A$

Where,
Ftu = ultimate tensile strength,
Pmax = maximum load before failure,
A = average cross sectional area.

Stress vs strain curves were plotted to calculate tensile modulus. The line of least squares was fitted to the initial portion of the stress vs strain curve and the value of the slope of that line was assigned as tensile modulus.

4.4.4. Procedure for Short beam Shear test

Some modifications are suggested to the ASTM guidelines in making the specimens tested for calculating SBS. As quoted earlier, that as revised in the year 2000 the ASTM D 2344 test removes all the reference to the shear strength as being the property measured with a belief that along with shear, many other complex stress states are generated far from the mid-plane and energy is not utilized in pure shear failure. Research was done by independent researchers on the key parameters of this test in order to achieve a pure shear failure of the SBS specimen [100]. Span to thickness ratio in the range of 6 – 8 is suggested to be used for achieving shear failures. Span to thickness ratios in the range of 6.74-6.92 were used in this investigation. A full list of specimen dimensions for the 7 ply and 11 ply modified laminates are given in Appendix 1.

Specimens were loaded in a 3 point bending machine with a fixed span length of 36 mm. Load vs Load point displacement data was measured and maximum load observed during the test was used to calculate short beam strength of the specimen using the following equation:

$$F^{sbs} = (0.75*P_{max}) / (b*h)$$

Where,
P_{max} = maximum load before failure,
F^{sbs} = short beam strength,
b = specimen width and
h = specimen thickness.

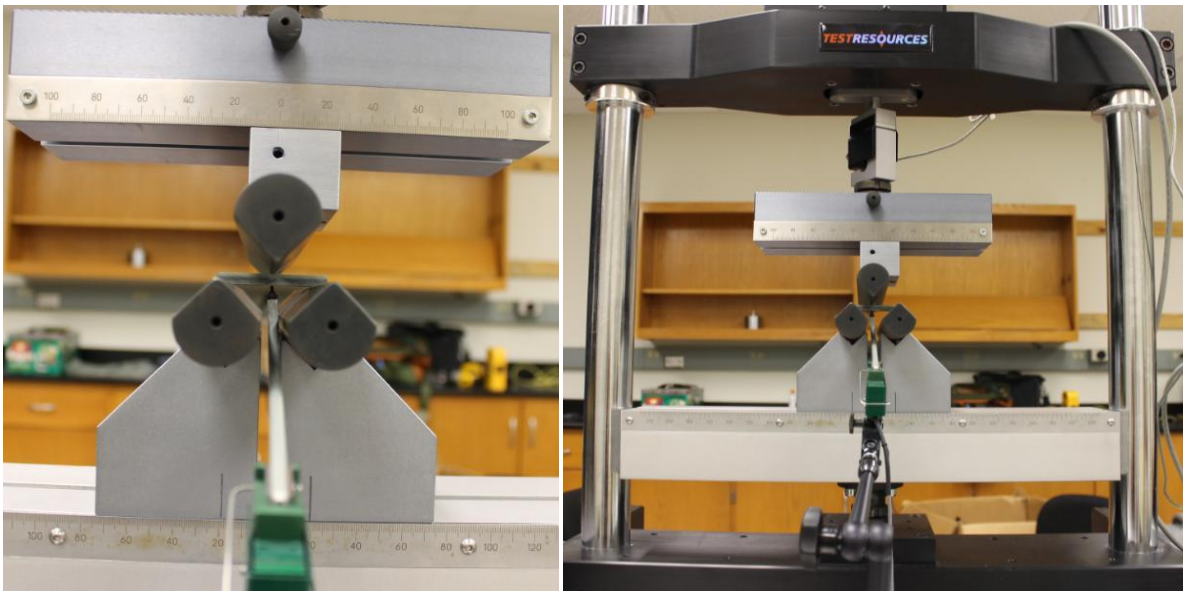

Figure 4-10: SBS Test Setup

4.4.5. Electrical Resistivity of CNT modified composite laminate

As specified in previous sections CNTs have excellent electrical properties. Since we are modifying individual laminate plies using aligned CNT sheets, the resultant laminate is expected to develop some electrical conductivity in comparison to the non-conductive glass-epoxy composite laminate. Agilent 34420A Micro Ohm Meter was used to measure the electrical resistance of the CNT modified specimen using four point probe method to avoid contact resistance which could be developed if two point probes would have been used. Electrical Resistance was measured in the fiber direction and the through thickness direction for the 12 ply composite laminate with all plies modified by the aligned CNT sheets in the parallel and perpendicular directions. Conductive silver epoxy paste and thin copper sheets

were used to make electrical contacts on the composite laminate required to make the four point probe contact.

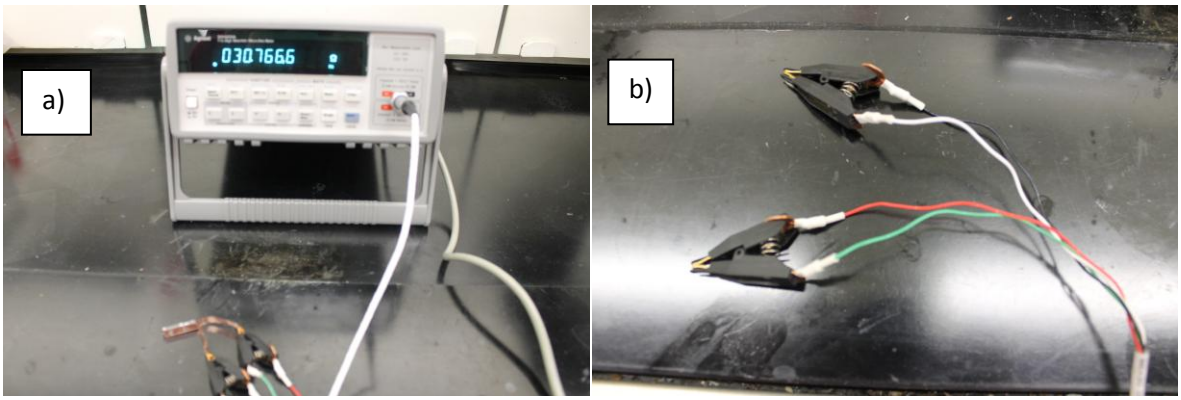

4-11: a) Electrical Resistance Measurement Test Setup; b) 4-point probe

Resistivity of individual specimens was then calculated using the measured resistance and the specimen dimensions as follows:

$$\rho = (R*A)/L;$$

Where,
ρ = resistivity,
R = Resistance,
A = cross-sectional area of the specimen and
L = length of the specimen.

Chapter 5 Results and Discussion

5.1.1. Mode I test results

Critical strain energy release rates are calculated using load vs load point displacement curves and '$C^{1/3}$ vs a' curve. G_{Ic} values were calculated at crack onset and for crack propagation. The plateau region was never achieved in the R-curve for all the specimens and the G_{Ic} values kept on increasing hence it was not possible to assign an average value to G_{Ic} propagation. Therefore only G_{Ic} initiation values were reported.

Load vs Load point displacement curves

The load vs load point displacement curve of a representative DCB specimen is shown in Figure 5.1. All load vs load point displacement curves are divided in to two parts: Linear part, where the crack is not propagated on the addition of excess load and Non-linear part, where the addition of excess load causes the crack to propagate. As seen in the Fig. repetitive small plateaus are observed in the non-linear part during crack extension followed by steep fall in the load values. They are observed when the energy available is not enough for extending the crack and additional energy is required for crack growth. Once enough energy builds up a sudden and rapid crack growth occurs which utilizes that built up energy and hence a fall in load value is witnessed.

Compliance Calibration

Compliance values of every tested specimen were calculated as a ratio of load point displacement to the load at a particular crack length. Compliance value was calculated at each marked point on the specimen meant to calculate crack length and cube root of compliance was plotted as a function of crack length to determine Δ. Δ was calculated by fitting line of least squares on this curve.

Table 5-1: Δ values of the representative DCB Specimen

Type	Δ (mm)
Control_4	29.61
2 Layer Parallel_1	21.21
2 Layer Perpendicular_6	20.44
4 Layer Perpendicular_5	31.16
8 Layer Perpendicular_4	23.68

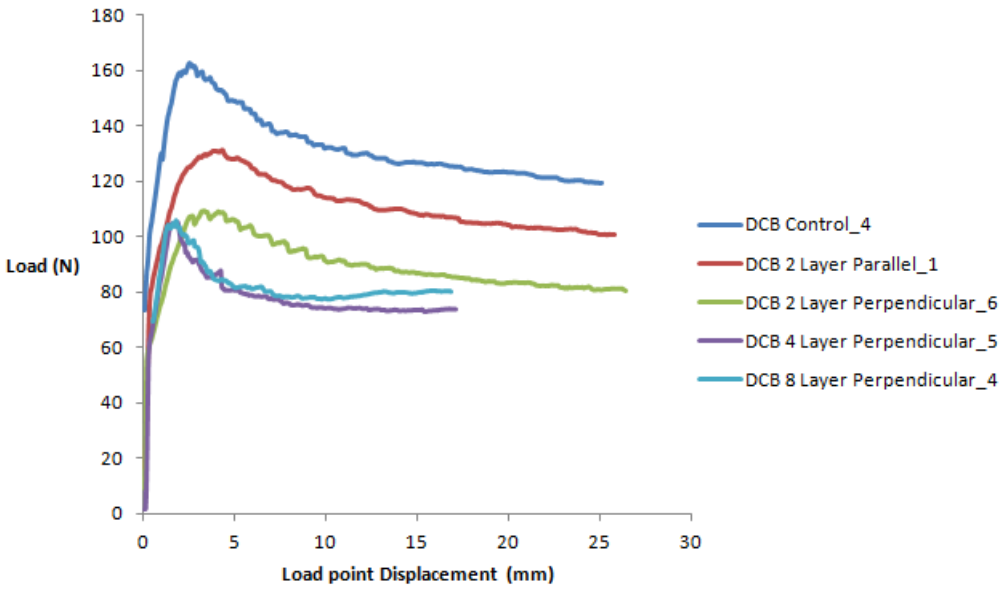

Figure 5-1: DCB Load vs Load point Displacement Curves of Representative Specimens

G_{Ic} Initiation Values

In order to eliminate operator errors in manually observing the crack growth, G_{Ic} values are calculated using Non-Linearity method as 5% offset method gives over-estimated values for G_{Ic} initiation. NL method is preferred for estimating failure criteria in damage tolerance analyses of structural laminates and is recommended by ASTM D 5528 for it being conservative. Table shows G_{Ic} initiation values of all the tested specimens.

G_{Ic} initiation value of the control specimen is seen to be in the range of state-of-the-art prepreg toughened systems [2]. The G_{Ic} initiation value of 4 and 8 layer perpendicular samples seemed to decrease by 46% and 48.66% respectively. An average increase of 18.63% and 23.95% was observed in the G_{Ic} initiation values for 2 layer perpendicular and parallel samples respectively.

Table 5-2: Calculated Average GIc Initiation values and percent change for DCB samples

Type	Mean	Standard Deviation	Percent Change %
Control	0.263	0.0029	-
2 Layers Parallel	0.326	0.0143	+23.95
2 Layers Perpendicular	0.312	0.1	+18.63
4 Layers Perpendicular	0.142	.009	-46.00
8 Layers Perpendicular	0.135	0.026	-48.66

R curves

Average G_{Ic} values were calculated for all the specimens in a sample and their relation with crack growth was plotted. It was seen that G_{Ic} values escalated quickly after

crack initiation. Fig. shows the R curves for all the tested samples. Usually, the G_{Ic} values stabilize on further crack propagation and after 10-20 mm of the crack growth the R curve enters into a plateau region. The R curves for our samples did not seem to enter a plateau region even after 70 mm of crack growth. The G_{Ic} values were always on an increase. This behavior was common for the control as well as CNT modified laminates. Hence a stable G_{Ic} propagation value could not be reported.

Mode I fracture Images – SEM:

SEM images of Mode I fractured surface of specimens from all types of samples are shown below. The specimens are cut to show the crack initiation and propagation surface from a = 0 mm - 3 mm. For control samples smooth interfacial surface was seen which proves bonding between the fibers and matrix is not strong. A thick sheet of CNT layer is seen on the fracture surface for the 4 and 8 layer perpendicular samples. However fractured CNTs and improved matrix rich regions were seen for 2 layer parallel and perpendicular samples.

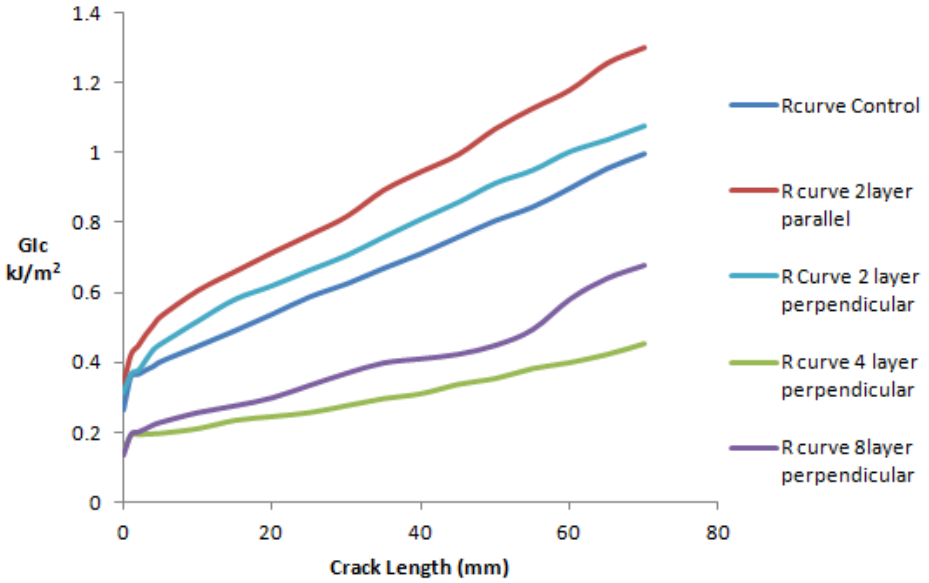

Figure 5-2: R Curves of representative Specimens

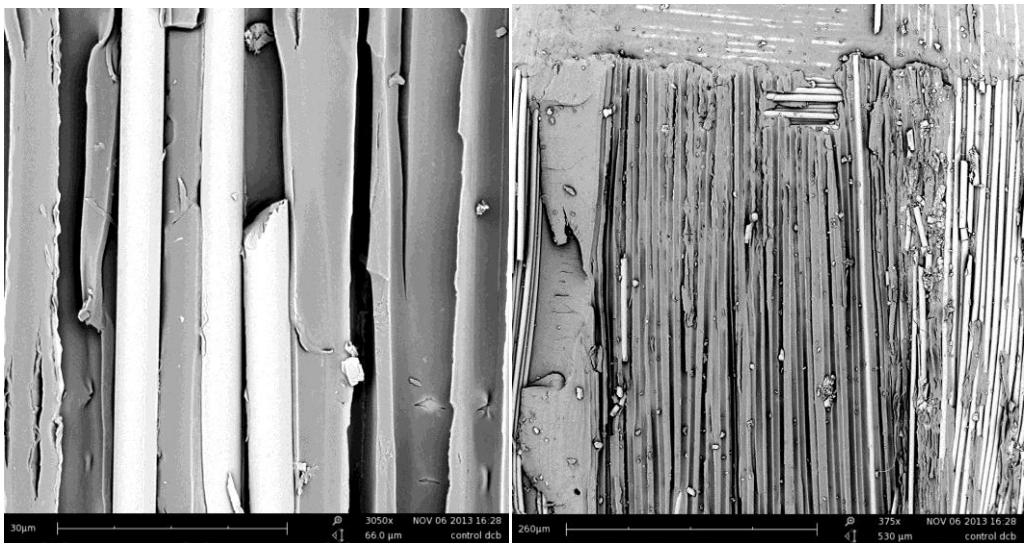

Figure 5-2: SEM Images of Control DCB Specimen at crack Initiation: (a) Fiber Matrix Interface; (b) Overview

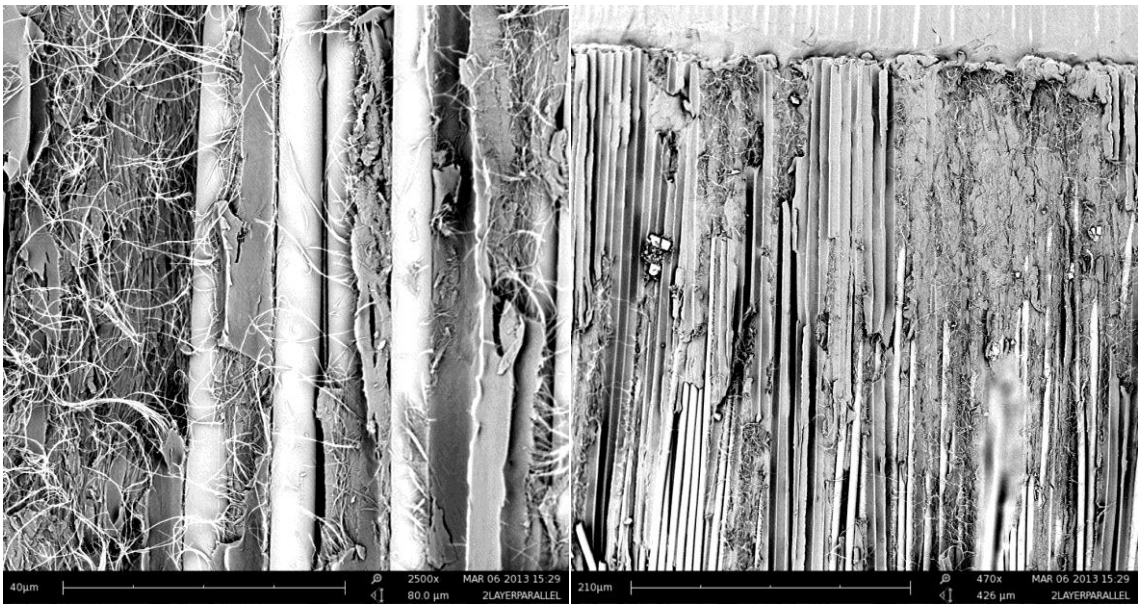

Figure 5-3: SEM Images of 2 Layer Parallel Specimen at crack Initiation: (a) Fiber Matrix Interface; (b) Overview

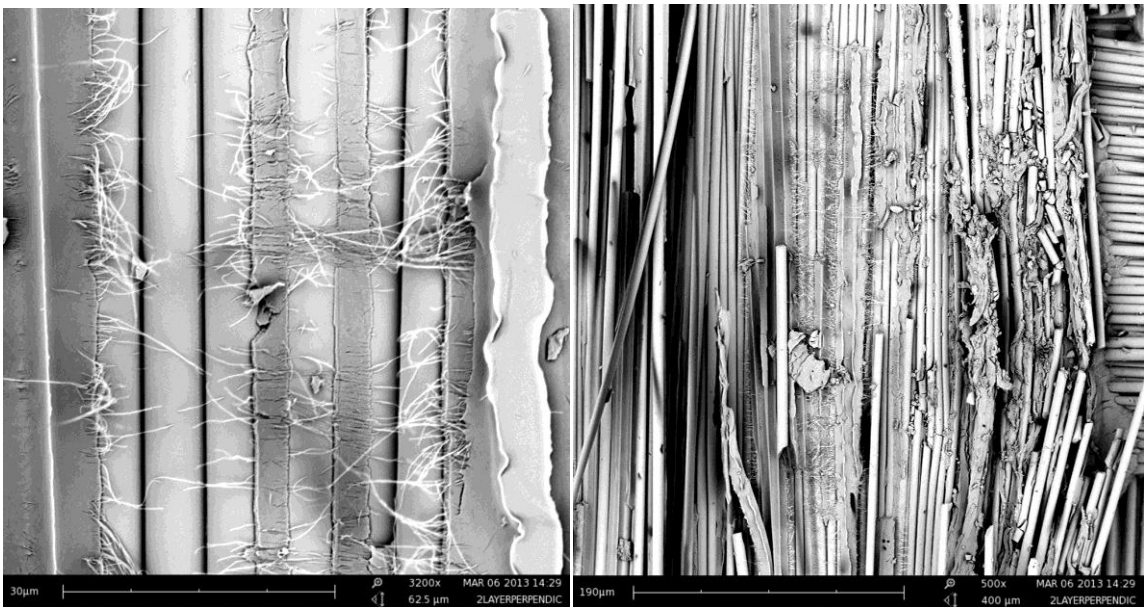

Figure 5-4: SEM Images of 2 Layer Perpendicular Specimens at Crack Initiation: (a) Fiber Matrix Interface; (b) Overview

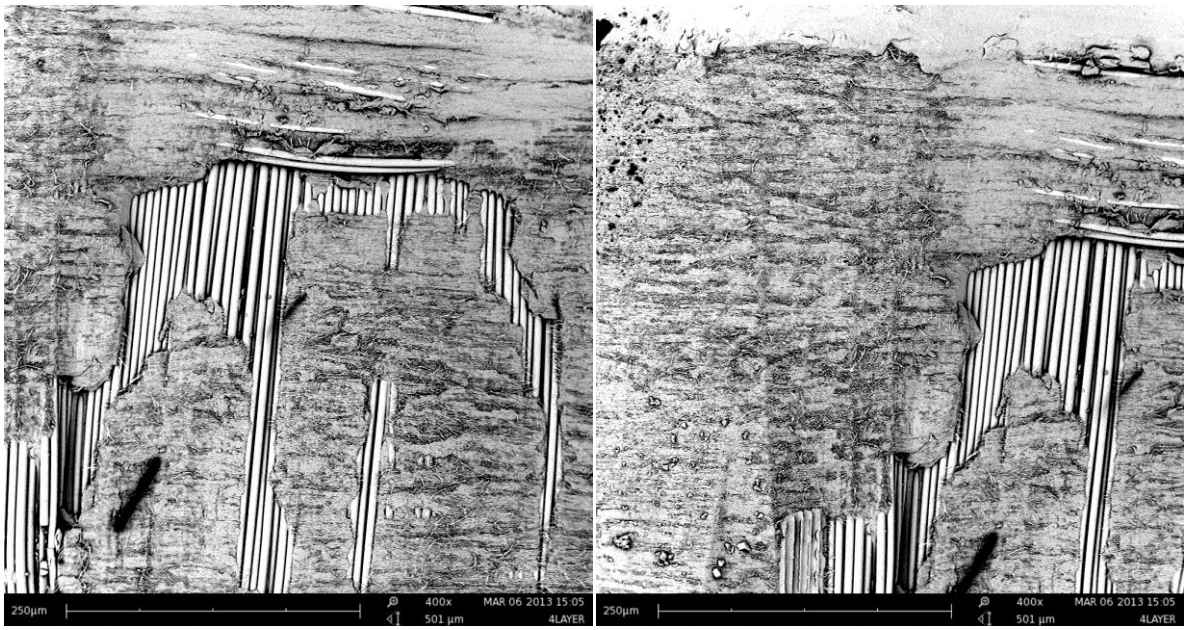

Figure 5-5: SEM Images of 4 Layer Perpendicular Specimen at crack Initiation: (a) Fiber Matrix Interface; (b) Overview

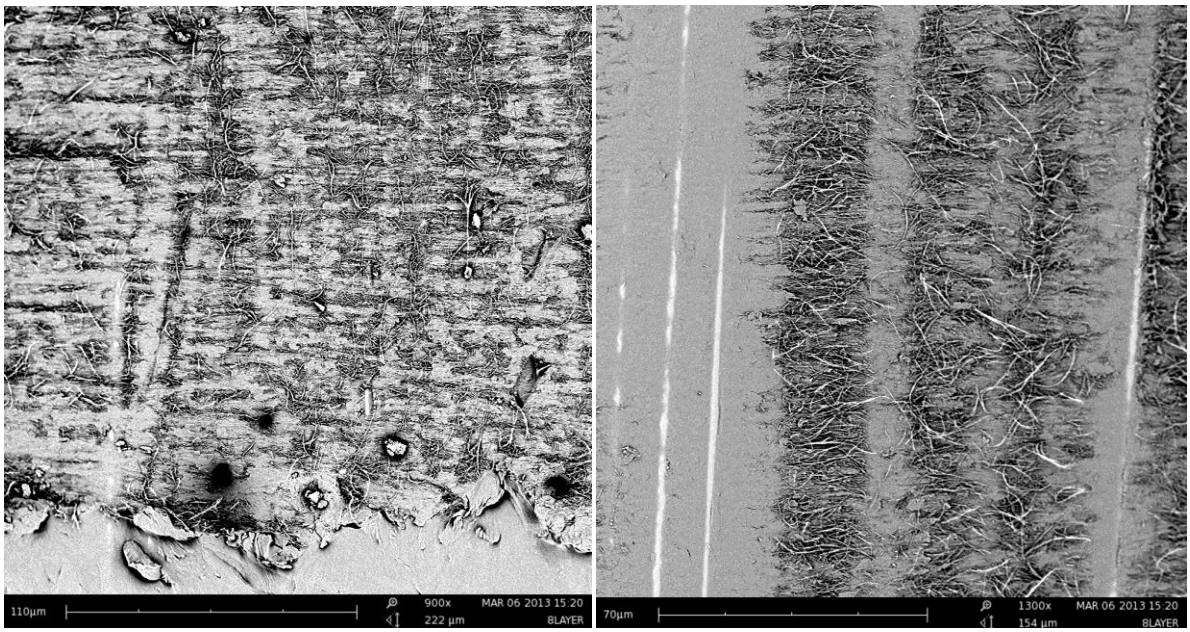

Figure 5-6: SEM Images of 8 Layer Perpendicular Specimen at crack Initiation: (a) Fiber Matrix Interface; (b) Overview

5.1.2. Discussion

Addition of aligned sheets of MWCNTs in between the plies affected the Mode I behavior significantly in both the positive and negative manner. Mechanisms responsible for improving MODE I fracture behavior are fiber-bridging, fiber-pullout, crack pinning, microcracking, crack bridging and crack path deflection. Initiation fracture toughness is dominated by matrix material's inherent toughness. An increase in the initiation fracture toughness therefore suggests that the aligned CNT sheets toughened the epoxy matrix in its vicinity at the mid-plane. SEM images of 4 and 8 Layer perpendicular samples show a thick layer of CNT sheet atop the glass fibers. This shows that excess amount of CNTs were introduced into the mid-plane which instead of toughening the laminate formed a thick CNT-reinforced layer of matrix through which the crack travelled easily without any macro fiber bridging taking place. Fiber bridging was evident in control samples which left smooth interfacial surface on the matrix behind; whereas dense fractured CNT network was seen around the fiber-matrix interface in the 2 Layered parallel and perpendicular samples, which was rough on the ends but smooth below. This shows that CNTs from the aligned sheet could not pass through the glass fiber layer along with the matrix onto adjacent layers. Due to this they could only improve the upper part of the interface and toughen it. As it is evident from the images, energy was also absorbed in mechanisms like crack bridging, CNT fiber rupture and pullout. Better results could have been expected if CNTs would have acted as z-reinforcements by flowing to the adjacent layers and had it improved the whole interface. The reason for that not being the case was the tangles and van der Waals forces present between the nanotubes which held them together while drawing.

5.2. Mode II Test Results:

Four Layer Perpendicular and Eight Layer Perpendicular samples showed the presence of excess nanotubes in the midplane and proved to significantly decrease the mode I toughness; thus were not made and tested using ENF. Control, 2 Layer Parallel and 2 Layer Perpendicular samples were tested using ENF test. Owing to the abrupt crack propagation achieved after the crack onset in ENF test, propagation values could not be determined. Therefore only G_{IIc} initiation value was calculated and reported.

Load vs Load point Displacement curves

A linear relationship was observed between the observed loads and the load point displacement. These curves had a characteristic transition in them displaying the deformation of the specimen going from the elastic to plastic region. Elementary beam theory suggests that a Mode II facture will propagate unstably if the ratio of initial crack length to half span length is smaller than 0.7 [] which is in accordance with our specimens. The ENF test was programmed to be terminated in case it measures a 50% drop in the recorded load. All the curves showed a linear behavior and ended at maximum load, suggesting every specimen had abrupt crack propagation. A set of representative curves is shown in figure 5.7.

Compliance Calibration

Compliance values are calculated as the inverse of the slope of Load vs Load point displacement curve. Here two compliance values were required: 1] Compliance of the Initial

Elastic portion and 2] Compliance for Initial Critical Load. To calculate these values, initial elastic part and the end part including maximum load of the the Load vs Load point displacement curve were plotted. Line of least squares was fitted on both the curves and the inverse of their slope was calculated to be respective compliance values. Fig. gives the representative curves used for calculating compliance.

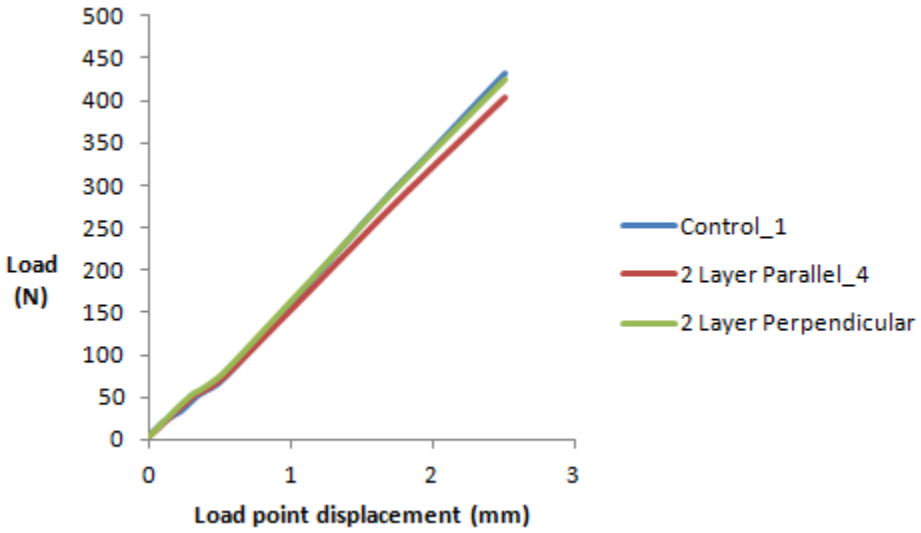

Figure 5-7: ENF Load vs Load point Displacement Curves

G_{IIc} Initiation Values

G_{IIc} initiation values are calculated using the two equations given in classical plate theory. Table gives the calculated values G_{IIc} initiation. The percentage increase given in the table is calculated with respect to that of control sample. Initiation value for Mode II type of fracture was almost double for the control sample in comparison to the Mode I value.

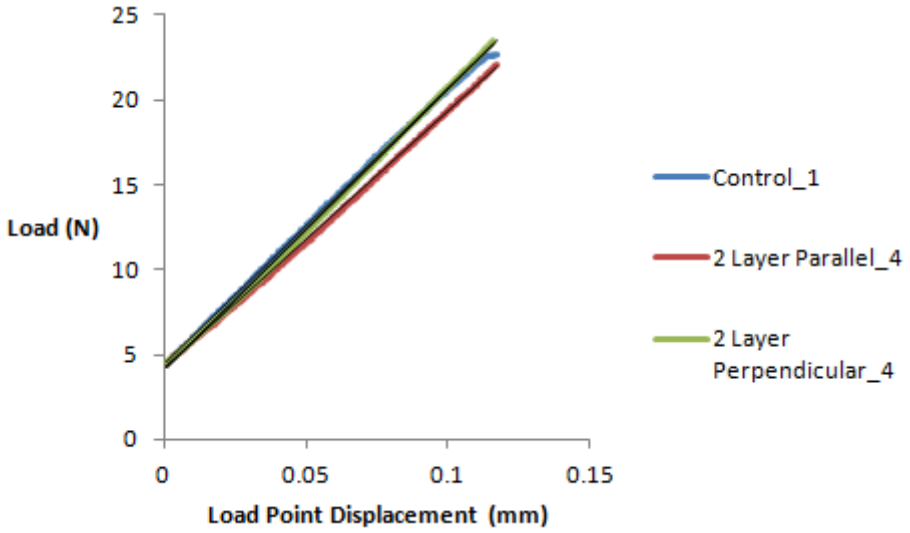

Figure 5-8: Representative ENF Load vs Displacement curves of Initial Elastic Portion

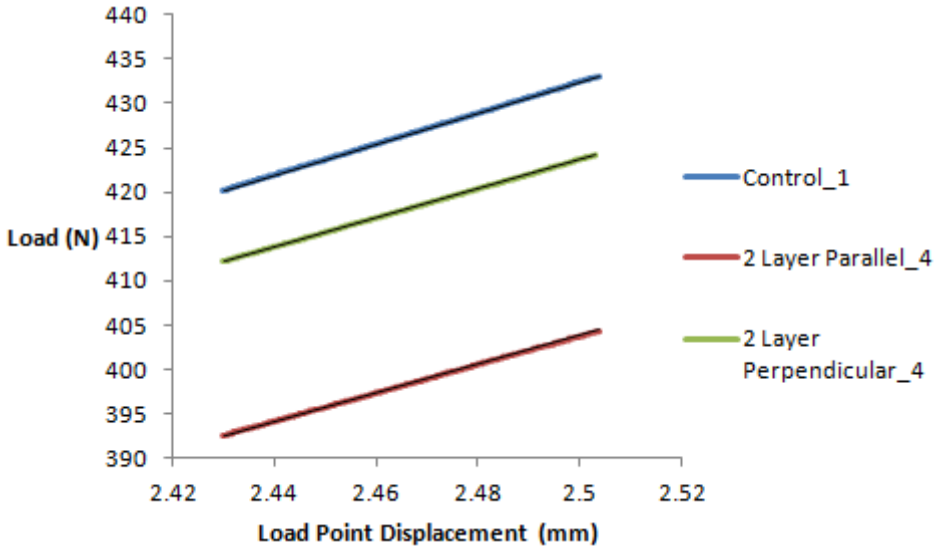

Figure 5-9: Representative ENF Load vs Displacement curves of Initial Critical Portion

This value was close to the state-of-the-art toughened epoxy prepreg system reported in literature [E-glass non crimp]. The calculated average G_{IIc} initiation value for the 2 Layer

Parallel sample seemed to reduce by 6.2 % whereas an increase of 17.13% was seen for 2 Layer Perpendicular Sample with respect to the average initiation value of control sample.

Table 5-3: Calculated Average GIIc Initiation values and percent change for ENF samples

G_{IIc} [kJ/m^2]			
Specimen No	Control	2 Layer Parallel	2 Layer Perpendicular
Mean	0.467	0.438	0.547
Standard Deviation	0.067	0.062	0.041
% Change	-	-6.2	17.13

Mode-II fracture Images – SEM

SEM images of Mode II fractured surface of specimens from all types of samples are shown below. The specimens are cut to show the crack initiation and the abrupt propagation surface from a=0 mm-3 mm. Smooth fiber-matrix interface was seen along with the presence of shear hackles for the control sample. CNT reinforced interface with comparable hackles were seen for 2 Layer Parallel sample. A lot more shear hackles were seen in the SEM image of 2 Layer Perpendicular sample.

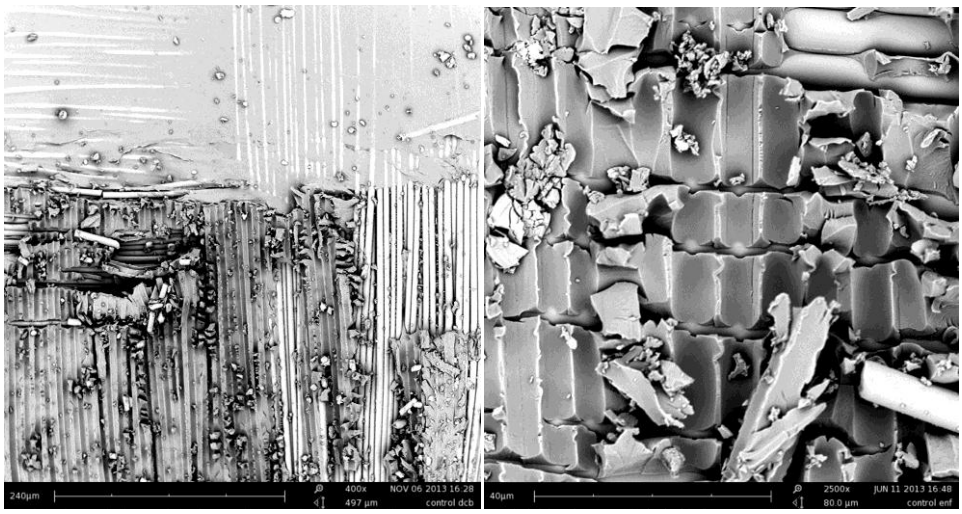

Figure 5-10: SEM Images of Control DCB Specimen at crack Initiation: (a) Overview; (b) Fiber Matrix Interface

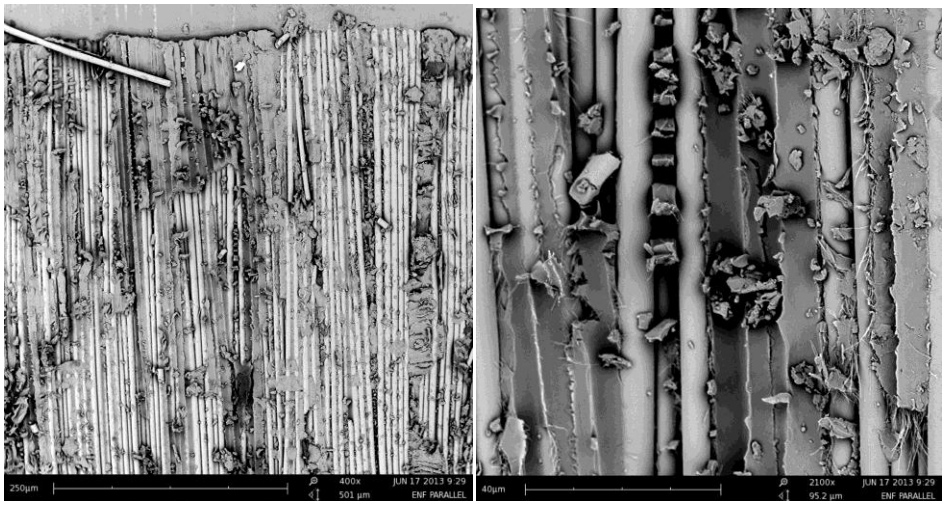

Figure 5-11: SEM Images of 2 Layer Parallel Specimen at crack Initiation: (a) Overview; (b) Fiber Matrix Interface

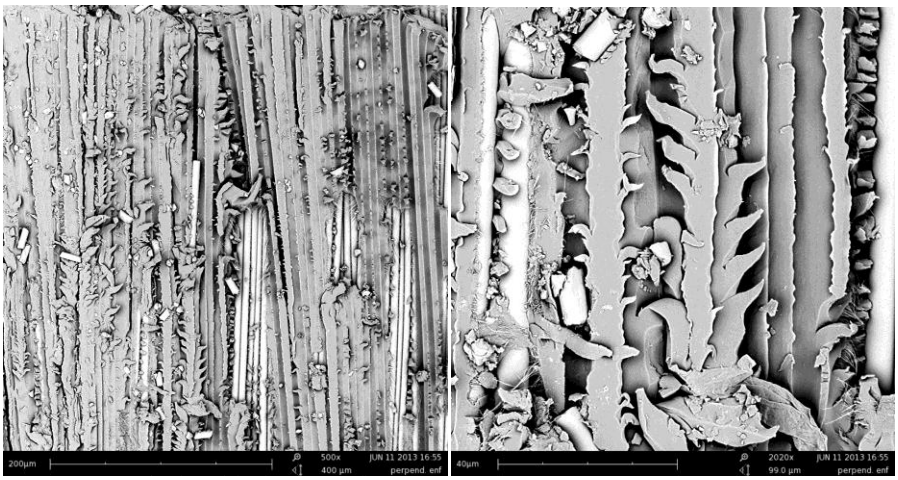

Figure 5-12: SEM Images of 2 Layer Perpendicular Specimen at crack Initiation: (a) Overview; (b) Fiber Matrix Interface

5.2.1. Discussion

Introduction of the aligned CNT sheet in the mid-plane of ENF sample gave mixed results for 2 Layer Parallel and Perpendicular samples. The mechanism majorly responsible for improving Mode II fracture behavior is shear yielding of matrix which results in formation of hackles at the fractured surface. Crack bridging does not play a decisive role here due to the nature of load applied and crack generated. CNT rupture and pull-out are seen in the SEM images but their occurrence with respect to the shear yielded resin hackles is minimal. The number of hackles seen in the SEM Image of 2 Layer Parallel sample is comparable to that seen in the control sample, but the size of hackles created in the latter seem to be larger than that of the former. The G_{IIc} initiation values of 2 Layer Parallel sample are lower by 6.2% than that of control sample. SEM images of 2 Layer Perpendicular sample shows larger and higher number of hackles formed as compared to both other samples along

with some of the CNT rupture and pull-out. This is the reason of 17.13% increase in the stress energy release rate of Mode II fracture at crack initiation with respect to that of control sample. Individual CNT ropes in an aligned sheet is also assumed to act as barrier present in the path of crack initiation and growth for the perpendicular direction which could require increased amount of energy to cross each barrier and hence more energy is dissipated overall before crack is initiated. Our results do seem to suggest this mechanism but it has not been proved.

5.3. Tensile Test Results

Stress at each data point was calculated using the load data and the specimen dimensions. Stress vs strain curves were plotted for each specimen and modulus was calculated from the slope of the line of least squares fitted on to those curves. Ultimate tensile strength was calculated using the maximum observed load value. Important thing to note was that despite all of the careful preparation of samples with tabs, the specimens failed near the lower tab.

Stress vs Strain curves

Calculated stresses were plotted against the measured strain values to get the stress vs strain curves. These curves showed a linear behavior between stress and strain followed by a steep drop in load values where the specimens failed. Similar curves were seen for all

the specimens of all types. Fig shows representative stress vs strain curves of 3 types of samples.

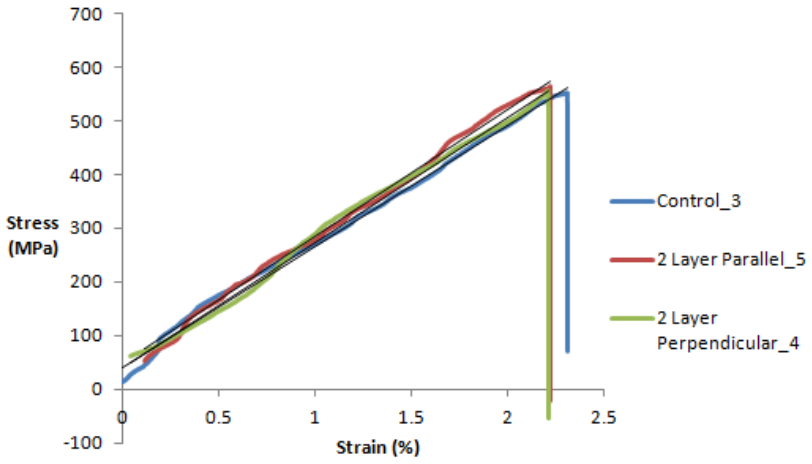

Figure 5-13: Tensile Stress vs Strain Curves of representative specimens

Mechanical Properties

Average ultimate tensile strength and modulus of all the specimens per sample were calculated. Following Table shows the ultimate tensile strength and modulus value of every tested specimen. No significant change in the magnitude of either property was seen for the CNT modified samples over the control sample.

5.3.1. Discussion

In-plane mechanical tests were performed in-order to verify the effect of aligned CNT sheets on the in-plane properties of the modified laminate. As shown in the literature,

the in-plane properties of a composite laminate is often compromised in order to improve the through thickness properties, which in turn limits the use of these through thickness reinforced laminates in the structural applications requiring the highest volume fractions. Improving the through thickness properties while keeping the in-plane properties intact should be the ideal case.

Table 5-4: Calculated Average Load, Tensile Strength and Modulus for Tensile Samples

Type	Specimen No.	P_{max} (N)	F^{tu} (MPa)	E (GPa)
Control	Mean	24730.73	556.86	23.308
	STD	668.34	12.52	2.16
2 Layer Parallel	Mean	24153.44	557.285	23.775
	STD	437.77	11.74	2.19
2 Layer Perpendicular	Mean	23959.38	561.167	24.008
	STD	883.46	19.82	2.83

Here we know that all the tensile samples failed near the tabbed region in spite of the efforts taken to prevent them from failing near the tabs. Even though, comparable results were seen for all the samples and we could compare their performance owing to similar failure modes for all. We can conclude that the in-plane properties were not compromised. It was not surprising that we did not see an increase in the in-plane properties because the overall fraction of the CNTs in the sample was very small.

Further testing could be done with further preventive measures like reducing the thickness of the laminate, using a tapered tab angle instead of using 90^o as the tabbing angle

and reducing the height of the specimen to gain more confidence in stating the above mentioned result.

5.4. Short Beam Strength Results

Measured load values were plotted against the load point displacement values to get the load vs load point displacement curves for the control and the 2 layer parallel and perpendicular 7 and 11 plies CNT modified samples. Maximum load observed during the test was used to calculate the short beam strength of each specimen.

Load vs Load point displacement curves

Curves of similar nature were seen for all type of samples. Similar to the tensile test data, the drop in the observed load after specimen failure was seen. Following figure shows the representative curves for the control and 7 ply and 11 ply CNT modified laminates.

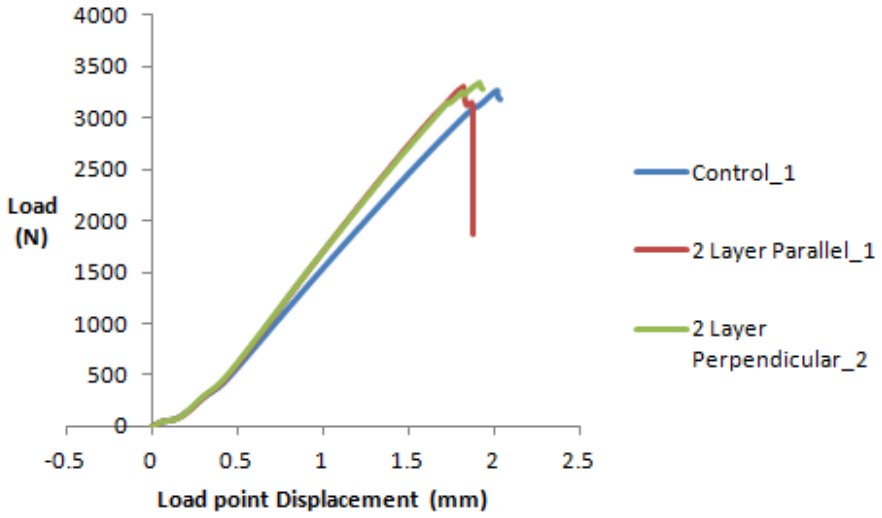

Figure 5-14: SBS Load vs Load point Displacement Curves for 11 Plies CNT Modified laminates

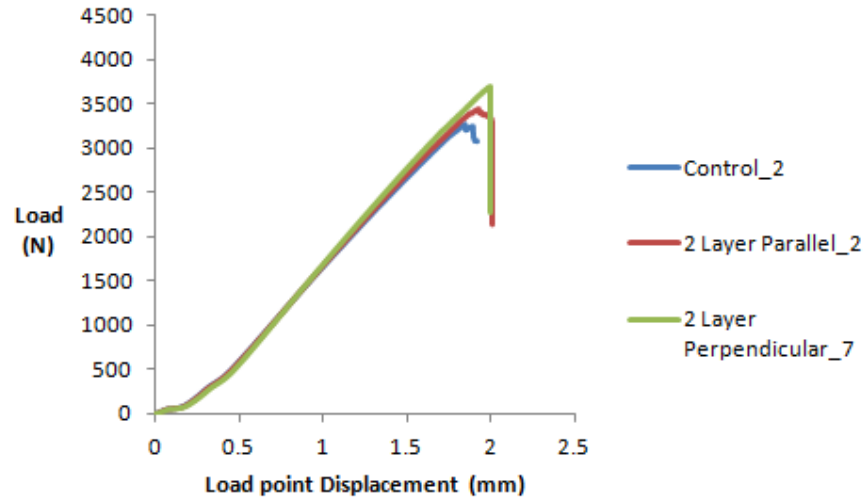

Figure 5-15: SBS Load vs Load point Displacement Curves for 7 Plies CNT Modified laminates

Short beam strength

Short beam strength was calculated using the maximum load observed in the load vs load point displacement curves. It was observed that the assumed shear failure in the SBS

specimens did not occur at the specimen mid-plane. The failure occurred close to the 1/3rd thickness from one edge of the specimen. The 2 Layer Parallel sample specimens made by modifying 7 plies with CNT sheets did not fail in the CNT modified plies for most of its specimens whereas the 2 Layer perpendicular specimens did fail in the CNT modified plies. For the 11 ply CNT modified specimens, the failure for most of the specimens did occur in the CNT modified plies.

Short beam strengths of the 7 plies and 11 plies CNT modified laminates are given in Appendix 2. The results obtained were not significantly different for the 11 plies CNT modified laminates as compared to the control sample whereas 7.2% increase was seen in the maximum observed load and 2.6% increase in the short beam strength for the 2 Layer Perpendicular sample fabricated with 7 CNT modified plies as compared to the control sample. No significant difference in the short beam strength of 2 Layer Parallel sample with 7 CNT modified plies as compared to the control sample was observed, however the average values obtained for the former were seen to be lower than that of the control sample.

Table 5-5: Calculated Average Maximum Loads and Percent Increase for 7 ply CNT modified laminate samples

Maximum Load Observed (N) – 7 ply CNT modified laminate			
Specimen	Mean	Std Deviation	% Increase
Control	3423.46	180.51	-
2 Layer Parallel	3410.86	190.37	-
2 Layer Perpendicular	3669.86	109.36	7.19

Table 5-6: Calculated Average Maximum Loads and Percent Increase for 11 ply CNT modified laminate samples

Maximum Load Observed (N) – 11 ply CNT modified laminate			
Specimen	Mean	Std Deviation	% Increase
Control	3312.09	110.25	-
2 Layer Parallel	3241.23	88.26	-
2 Layer Perpendicular	3279.03	69.85	-

Table 5-7: Calculated Average Short Beam Strengths and Percent Increase for 7 ply CNT modified laminate samples

Short Beam Strength (MPa) – 7 ply CNT modified laminate			
Specimen	Mean	Std Deviation	% Increase
Control	44.93	1.43	-
2 Layer Parallel	45.39	2.35	-
2 Layer Perpendicular	46.11	0.94	2.62

Table 5-8: Calculated Average Short Beam Strengths and Percent Increase for 11 ply CNT modified laminate samples

Short Beam Strength (MPa) – 11 ply CNT modified laminate			
Specimen	Mean	Std Deviation	% Increase
Control	44.91	0.977	-
2 Layer Parallel	44.05	0.959	-
2 Layer Perpendicular	44.41	1.123	-

5.4.1. Discussion

Toughened resin and improved fiber-matrix interface will help increase the measured short beam strength value. As discussed in the DCB and ENF test, our method is capable of modifying the fiber-matrix interface in the CNT modified plies but due to the sheet structure our nanotubes are not able to flow with matrix and hence they cannot cover and improve the interface for the whole glass fiber tow. Our CNTs do fill the resin rich regions and toughen them. Hence a moderate increase in the Short Beam Strength value of

CNT modified specimen is expected. Since the shear failure observed for 2 Layer parallel specimens with 7 CNT modified plies were not in the CNT modified ply, no significant change was recorded in comparison to control sample whereas improvement was seen in the 2 Layer perpendicular specimens with 7 CNT modified plies where the fracture did occur in the CNT modified plies.

Results observed for SBS specimens with 11 CNT modified plies were un-expected. This could be attributed to the loss of vacuum during the initial consolidation and temperature ramp up while fabricating the sample. After the sample was removed from the hot press, it was observed that the vacuum pipe along with the sealent tape came off the steel plate one-sided mold and the system was not in vacuum. This flaw during the sample fabrication could be the reason for not achieving any improvements in the short beam strength of 11 CNT modified plies SBS specimens.

5.5. Electrical Resistivity Results

Three set of specimens were tested for measuring the electrical resistance of the CNT modified composite laminates. Long and short specimens were used in the fiber direction for measuring the consistency in the results.

Table 5-9: Calculated Resistance and Resistivity of the CNT modified composite laminates

	Aligned CNT Sheet Direction	Electrical Resistance (kΩ)	Resistivity (kΩmm)
Fiber Direction - Long Specimen	Parallel	0.183	0.038
	Perpendicular	8.005	1.651
Fiber Direction - Short Specimen	Parallel	0.183	0.047
	Perpendicular	5.671	1.309
Through Thickness Direction	Parallel	0.01185	0.761
	Perpendicular	0.03114	1.95

5.5.1. Discussion

The resistivity results obtained were as expected. The electrical resistivity for the parallel aligned CNT sheet modified composite laminate specimens was lower than that of perpendicular aligned CNT sheet modified composite laminate specimens in the order of 30-50. This is attributed to the anisotropic CNT properties, preferred in its axial direction. Other speculated reason for higher electrical resistance is a possibility of CNTs losing contact due to imperfect CNT sheet placement for the perpendicular aligned CNT sheet during fabrication.

We could also measure electrical resistance values in the through thickness direction close to that of the perpendicular aligned CNT sheet modified composite laminate specimens. This confirms that the CNTs present in the laminate do modify half of the fiber-matrix interface and if the adjacent plies are modified with aligned CNT sheets, CNTs from each side of the ply migrate to an extent in the z-direction and make contact with the CNTs present on the other side of the ply. Thus it is observed that our CNT modified specimens achieve better in-plane and through thickness electrical properties.

Chapter 6 Conclusion

Drawable MWCNT arrays were synthesized in a low pressure chemical vapor deposition system with iron chloride as a vapor phase catalyst and quartz substrate. MWCNT arrays were successfully drawn throughout the substrate width to achieve aligned CNT sheets. . Uniform CNT sheet placement throughout the laminate is achieved with active control over CNT location and 2D orientation for incorporating CNTs into bulk laminate irrespective of the fiber-matrix system used.

As drawn aligned CNT sheets are then laid onto the woven glass fiber reinforced epoxy matrix prepreg plies which are stacked symmetrically followed by consolidation and curing to form CNT modified composite laminates. Use of optimized amount of CNT sheets showed improvements in the initiation interlaminar fracture toughness which is one of the most significant limitations of 2D composite laminates. Very little improvements are seen in the short beam strength of the CNT modified composite laminates and the in-plane mechanical properties of the CNT modified composite laminates were not compromised in order to improve their through thickness properties.

Modifying the composite laminate with aligned CNT sheets imparted the in-plane and the through thickness electrical properties to the initial non-conductive glass-epoxy composite laminate. Laminates with aligned CNT sheets parallel to the fiber direction showed lower electrical resistance than those with CNT sheets perpendicular to the fiber-direction.

The improvement in the through thickness properties achieved is attributed to various mechanisms like toughening of matrix achieved by the presence of nanotubes, CNT-crack bridging, fracture and pull-out and partly improved fiber-matrix interface.

The improvement seen could have been better had the CNTs from the sheet penetrated deeper through the modified plies on to the adjacent plies, thus reinforcing the whole fiber matrix interface. One restraint to that was the CNT sheet structure used. The tangles and van der Waals force which made the CNT array drawable, held individual CNTs tight enough not to allow them to penetrate freely. Other and the major restraint was the form of matrix used. The prepreg had the epoxy matrix in B-stage where the viscosity of the resin is high and it does not have to flow to cover the whole fabric. Poor penetration of the CNT network was apparent in the SEM images of the fractured CNT modified specimens where long and bundled resin free CNT fragments are seen.

Recommended Future Work

To achieve better improvements in the through thickness direction, we would like to repeat the set of DCB and ENF tests using specimens with modified adjacent plies along with the mid-plane. We believe that a completely reinforced fiber-matrix interface would be able to resist the delamination better than the current partially modified fiber matrix interface at the mid-plane.

We would also want to achieve the potential through thickness improvements with the as developed CNT structure by achieving a deeply penetrated CNT network. Vacuum Assisted Resin Transfer Molding (VARTM) method would be preferred to fabricate aligned

CNT sheet modified composite laminates. 8HS Woven Glass fabrics covered with aligned CNT sheets would be reinforced using A-stage epoxy matrix. Modifiers would be used to lower the viscosity of the matrix system. Resin flow through the Fiber-CNT system would force the compliant CNT sheet structure to penetrate onto the adjacent plies through the glass fiber tows thus reinforcing the laminate in z-direction.

We would also like to use the imparted electrical property of the modified laminate by fabricating them as structural strain sensors. Experiments on standardizing the drawable VACNT array would be carried out to achieve consistent electrical and mechanical properties in every batch will be the primary focus.

REFERENCES

[1] V. Alveraz, C.R. Bernal and P.M. Fonrtini, "The influence of matrix chemical structure on the mode I and II interlaminar fracture toughness of glass-fiber/epoxy composites," Polym Compos., 24 (2003) 140-148.

[2] A. T.Seyhan, M. Tanoglu and K. Schulte, "Mode I and mode II fracture toughness of E-glass non-crimp fabric/carbon nanotube (CNT) modified polymer based composites," Engineering Fracture Mechanics, 75 (2008) 5151-5162.

[3] J. Kong, N. Franklin, C. Zhou, M. Chapline, S. Peng, K. Cho and H. Dai, "Nanotube molecular wires as chemical sensors," Science 287 (2000) 622-625.

[4] C. Dekker, "Carbon nanotubes as molecular quantum wires," Physics Today, 52 (1999) 22-28.

[5] S. Peng, J. O'Keeffe, C. Wei, K. Cho, J. Kong, R. Chen, N. Franklin and H. Dai, "Carbon nanotube chemical and mechanical sensors," In: Proc. 3rd Int. Workshop on Structural Health Monitoring, (2001) 1-8.

[6] E. Thostenson and T. Chou, "Carbon nanotube networks: sensing of distributed strain and damage for life prediction and self healing," Adv. Mater., 18 (2006) 2837-2841.

[7] F. H. Gojny and K. Schulte, "Functionalization effect on thermo-mechanical behavior of multiwalled carbon nanotube/epoxy composites," Compos. Sci. Technol., 34 (2004) 2303-2308.

[8] F. H. Gojny, M.H.G. Wichmann, U. Kopke, B. Fiedler and K. Schulte, "Carbon nanotube-reinforced epoxy composites: enhanced stiffness and fracture toughness at low nanotube content," Compos. Sci. Technol., 34 (2004) 2363-2371.

[9] F. H. Gojny, M.H.G. Wichmann, B. Fiedler, W. Bauhofer and K. Schulte, "Influence of nano-modification on the mechanical and electrical properties of conventional fiber reinforced composites," Compos. A. Appl. Sci., 36 (2005) 1525-1535.

[10] A.T.Seyhan, F.H. Gojny, M. Tanoglu and K. Schulte, "Critical aspects related to processing of carbon nanotube/vinyl ester-polyester suspensions and their nanocomposites," Eur. Polym., J43 (2007) 374-379.

[11] W.H.G. Wichmann, J. Sumfleth, F.H. Gojny, M. Quaresimin, B. Fiedler and K. Schulte, "Glass fiber reinforced composites with enhanced mechanical and electrical properties – benefits and limitations of a nanoparticle modified matrix," Engng. Fract. Mech., 73 (2006) 2346-2359.

[12] V.P. Veedu, A. Cao, X. Li, K. Ma, C. Soldano, S. Kar, P.M. Ajayan and M.N. Ghasemi-Nejhad, "Multifunctional composites using reinforced laminae with carbon-nanotube forests," Nature, 5 (2006) 457-462.

[13] E.J. Garcia, B.L. Wardle, A.J. Hart and N. Yamamoto, "Fabrication and multifunctional properties of a hybrid laminate with aligned carbon nanotubes grown in situ," Compos. Sci. Technol. 68 (2008) 2034-2041.

[14] T.W. Ebbesen, H.J.Lezec, H. Hiura, J.W. Bennett, H.F. Ghaemi and T. Thio, "Electrical conductivity of individual carbon nanotubes," Nature, 382 (1996) 54-56.

[15] S. Berber, Y. Kwon, and D. Tomanek, "Unusually high thermal conductivity of carbon nanotubes," Phys rev lettrs, 84 (2000) 4613-4616.

[16] S. Ijima, "Helical Microtubules of Graphitic Carbon," Nature, 354 (1991) 56-58.

[17] C.H. Olk and J.P. Heremans, "Scanning tunneling spectroscopy of carbon nanotubes," J. mater. Res. 9 (1994) 259-262.

[18] M.S. Dresselhaus and M. Endo, "Relation of Carbon Nanotubes to Other Carbon materials," In M.S. Dresselhaus, G. Dresselhaus, Ph. Avouris (Eds): Carbon nanotubes, Topics Appl. Phys. 80 (2001) 11-28.

[19] M.S. Dresselhaus and Ph. Avouris, "Introduction to Carbon materials Research," In M.S. Dresselhaus, G. Dresselhaus, Ph. Avouris (Eds): Carbon nanotubes, Topics Appl. Phys. 80 (2001) 1-9

[20] J.P. Lu, "Elastic properties of carbon nanotubes and nanoropes," Phys. Rev.Lett. 79 (1997) 1297-1300.

[21] C. Li and T.W. Chou, "Elastic moduli of multi-walled carbon nanotubes and the effect of van der Waals forces," Compos. Sci. Technol., 63 (2003) 1517-1524.

[22] M.M.J. Treacy, T.W. Ebbesen and J.M.Gibson, "Exceptionally high Young's modulus observed for individual carbon nanotubes," Nature 381 (1996) 678-680.

[23] M. Yu, O. Lourie, M.J. Dyer, T.F. Kelly and R.S. Ruoff, “Strength and breaking mechanism of multiwalled carbon nanotubes under tensile load,” Science, 389 (1999) 582-584.

[24] J.P. Salvetat, A.J. Kulik, J.M. Bonard, G.A.D. Briggs, T. Stockli and K. Metenier, “Elastic modulus of ordered and disordered multiwalled carbon nanotubes,” Adv. Mater. 11 (1999) 161-165.

[25] T.W. Ebbesen and P.M. Ajayan, “Large scale synthesis of carbon nanotubes,” Nature, 358 (1992) 220-222.

[26] C. Journet, W.K. Maser, P.Bernier, A. Loiseau, M.L. Dellachapelle, S. Lefrant, P. Deniard, R. Lee and J.E. Fischer, “Large-scale production of single-walled carbon nanotubes by the electric-arc technique,” Nature, 388 (1997) 756-758.

[27] D.S. Bethune, C.H. Kiang, M. DeVries, G. Gorman, R. Savoy, J. Vazquez and R. Beyers, “Cobalt-catalysed growth of carbon tubes with single-atomic-layer walls,” Nature, 363 (1993) 605-607

[28] A. Thess, R. Lee, P. nikolaev, H. Dai, P. Petit, J. Robert, C.H. Xu, Y.H. Lee, S.G. Kim, A.G. Rinzler, D.T.Colbert, G.E. Scuseria, D. Tomanek, J.E. Fischer and R.E.Smalley, “Crystalline ropes of metallic carbon nanotubes,” Science, 273 (1996) 483-487.

[29] T. Guillard, S. Cetout, G. Flamant, and D. Laplaze, “Solar production of carbon nanotubes: structure evolution with experimental conditions,” J. Mater. Sci. Lett., 19 (2000) 511-514.

[30] P.M. Ajayan, “Nanotubes from carbon,” Chem. Rev. 99 (1999) 1787-1799.

[31] H. Dai, “Nanotube Growth and Characterization,” In M.S. Dresselhaus, G. Dresselhaus, Ph. Avouris (Eds): Carbon nanotubes, Topics Appl. Phys. 80 (2001) 29-53.

[32] Y. Yun, V. Shanov, Y. Tu S. Subramanium and M.J. Schulz, “Growth Mechanism of Long Aligned Multiwall Carbon Nanotube Arrays by Water-Assisted Chemical Vapor Deposition,” J. Phys. Chem. B, 110 (2006) 23920-23925.

[33] E. Couteau, K. Hernadi, J.W. Seo, L. Thien-Nga, Cs. Miko, R. Gaal and L. Forro, “CVD synthesis of high-purity multiwalled carbon nanotubes using $CaCO_3$ catalyst support for large-scale production,” Chem. Phys. Lett., 378 (2003) 9-17.

[34] Q. Zhang, D.G. Wang, J.Q. Huang, W.P. Zhou. G.H. Luo, W.Z. Qian and F. Wei, “Dry spinning yarns from vertically aligned carbon nanotube arrays produced by an improved floating catalyst chemical vapor deposition method,” Carbon, 48 (2010) 2855-2861.

[35] J. Kong, A.M. Cassell and H. Dai, “Chemical vapor deposition of methane for single-walled carbon nanotubes,” Chem.Phys. Lett. 292 (1998) 567-574.

[36] Y. Li, X.B. Zhang, X.Y. Tao, J.M. Xu, W.Z. Huang, J.H. Luo, Z.Q. Luo, T. Li, F. Liu, Y. Bao and H.J. Geise, “Mass production of high-quality multi-walled carbon nanotube bundles on a Ni/Mo/MgO catalyst,” Carbon, 43 (2005) 295-301.

[37] Y. Inoue, K. Kakihata, Y. Hirono, T. Horie, A. Ishida and H. Mimura, “One-step grown aligned bulk carbon nanotubes by chloride mediated chemical vapor deposition,” Appl. Phys. Lett., 92 (2008) 213113.

[38] Q. Li, X. Zhang, R. F. DePaula, L. Zheng, Y. Zhao, L. Stan, T.G. Holesinger, P.N. Arendt, D.E. Peterson and Y.T. Zhu, “Sustained Growth of Ultralong Carbon nanotube Arrays for Fiber Spinning,” Adv. Mater., 18 (2006) 3160-3163.

[39] S. Fan, M. Chapline, N. Franklin, T. Tombler, A.Casell and H. Dai, “Self-Oriented Regular Arrays of Carbon nanotubes and Their Field Emission Properties,” Science, 283 (1999) 512-514.

[40] H. Dai, J. Kong, C. Zhou, N. Franklin, T. Tombler, A. Cassell, S. Fan and M. Chapline, “Controlled chemical routes to nanotube architectures, physics and devices,” J. Phys. Chem. 103 (1999) 11246-11255

[41] D.J. Elder, R.S. Thomson, M.Q. Nguyen and M.L. Scott, “Review of delamination predictive methods for low speed impact of composite laminates,” Composite Structures, 66 (2004) 677-683.

[42] J.K. Kim and M.L. Sham, “Impact and delamination failure of woven-fabric composites,” Compos. Sci.and Technol., 60 (2000) 745-761.

[43] A.C. Garg, “DELAMINATION – A DAMAGE MODE IN COMPOSITE STRUCTURES,” Engng. Fract. Mech., 29 (1988) 557-584.

[44] T.K. O'Brien, "INTERLAMINAR FRACTURE OF COMPOSITES," NASA-Tm-85768 (1984).

[45] N. Sela an O. Ishai, "Interlaminar fracture toughness and toughening of laminated composite materials: a review," Composites, 20 (1989) 423-435.

[46] A.S.D. Wang, "Fracture Mechanics of sublaminate cracks in composite materials," Compos. Technol. Rev. 6 (1984) 45-62.

[47] D.J. Wilkins, J.R. Eisenmann, R.A. Camin, W.S. Margolis and R.A. Benson, ASTM STP, 775 (1982) 168-183.

[48] C.T. Herakovich, "Mechanics of fibrous composites," (1998) New York: Wiley.

[49] R.Y. Kim, "A technique for prevention of delamination," AFWAL-TR-82-4007, (1982) 218-230.

[50] W.J. Gilwee an Z. Nir, "Toughened reinforced epoxy composites with brominated polymeric additives," US Patent 6-493865 (1983)

[51] P.S. Sampath, V. Murugesan, M. Sarojadevi and G. Thanigaiyarasu, "Mode I and Mode II Delamination Resistance and Mechanical Properties of Woven Glass/Epoxy- PU IPN Composites," Polym. Compos. (2008) 1227-1234.

[52] A.F. Yee, "Modified matrix materials for tougher composites," ASTM Toughened Composite Symposium, (1985).

[53] A.P. Mouritz, “Review of z-pinned composite laminates,” Composites: Part A, 38 (2007) 2383-2397.

[54] J.S. Boyce, G.A. Freitas, C.L. Magee, T.M. Fusco, J.J. Harris and E. Kunkle, “Ultrasonic fastening system and method,” Patent WO 98/29243 (1998)

[55] I.K. Partridge, D.D.R. Cartie, M. Troulis, M. Grassi and X. Zhang, “Evaluating the mechanical effectiveness of z-Pinning,” In: Proceedings of the SAMPE technical conference, (2004)

[56] K.L. Rugg, B.N. Cox and R. Massabo, “Mixed mode delamination of polymer composite laminates reinforced through the thickness by z-fibers,” Composites, 33 (2002) 177-190.

[57] G. Freitas, C Magee, P. Dardzinski and T. Fusco, “Fiber insertion process for improved damage tolerance in aircraft laminates,” J. Adv. Mater., 25 (1994) 36-43.

[58] M. Grassi, X. Zhang and M. Meo, “Prediction of stiffness and stresses in z-fibre reinforced composite laminates,” Composites: Part A, 33 (2002) 1653-1664.

[59] K.L. Rugg, B.N. Cox, K.E. Ward and G.O. Sherrick, “Damage mechanisms for angled through-thickness rod reinforcement in carbon-epoxy laminates,” Composites: Part A, 29 (1998) 1603-1613.

[60] P. Chang, A.P. Mouritz and B.N. Cox, “Flexural properties of z-pinned laminates,” Composites: Part A, 38 (2007) 224-251.

[61] P. Chang, A.P. Mouritz and B.N. Cox, “Properties and failure mechanisms of z-pinned laminates in monotonic and cyclic tension,” Composites: Part A, 37 (2006) 1501-1513.

[62] C.A. Steeves and N.A. Fleck, “In-plane properties of composite laminates with through thickness pin reinforcement,” Int.J.Solids Struct., 43 (2006) 3197-3212.

[63] H.B. Holt, “Future composite aircraft structures may be sewn together,” Automotive Engineering, 90 (1992) 46-49.

[64] E. Wu and J. Liau, “Impact of unstitched and stitched laminates by line loading,” J. Compos. Mater., 28 (1994)

[65] T.J. Kang and S.H. Lee, “Effect of stitching on the mechanical and impact properties of woven laminate composite,” J. Compos. Mater., 28 (1994)

[66] L.K. Jain and Y.W. Mai, “On the effect of stitching on Mode I delamination toughness of laminated composites,” Compos. Sci. & Technol. 51 (1994)

[67] L.K. Jain and Y.W. Mai, “Analysis of stitched laminate ENF specimens for interlaminar Mode II fracture toughness,” Int. J. Fract., 68 (1994)

[68] C. Cacho-Negrete, “Integral Composite Skin and Spar (ICSS) Study Program,” AFWAL-TR-82-3053, Flight Dynamics Laboratory, Wright Aeronautical Laboratories, Wright –Patterson Air Force Base, Ohio (1982)

[69] L. Tong, A.P. Mouritz and M.K. Bannister, “3D fibre reinforced polymer composites” (2002) Boston: Elsevier.

[70] M. He and B.N. Cox, "Crack bridging by through-thickness reinforcement in delaminating curved structures," Composites: part A, 29 (1998)

[71] R.J. Palmer, M.B. Dow and D.L. Smith, "Development of stitching reinforcement for transport wing panels," Proc. Of the 1st NASA Advanced Composites Technical Conference., Part 2 (1991) 621-646.

[72] L. Wenning, C. Guangming and Q. Xin,. Proc. Of the 38th Int. SAMPE Symposium (1993)

[73] A.P. Mouritz, C. Baini and I. Herszberg, "Mode I interlaminar fracture toughness properties of advanced textile fiberglass composites", Composites: Part A, 30 (1999) 859-870.

[74] A.B. Macander, R.M. Crane and E.T. Camponeschi, "Fabrication and mechanical properties of multi-dimensionally (X-D) braided composite materials," Composite Materials: Testing and Design (7 Conf.), ASTM STP 893, (1986) 422-443.

[75] V.A. Guenon, T.W. Chou and J.W. Gillespie, "Toughness properties of a three dimensional carbon-epoxy composite," J. Mater. Sci., 24 (1989) 4168-4175.

[76] F.J. Arendts, K. Drechler and J. Brandt, "Advanced textile structural composites – status and outlook," Proc. 13th Int. Conf. Comp. Mats., (2001)

[77] C.H. Liu, J. Byan and T.W. Chou, "Mode II interlaminar fracture toughness of three-dimensional textile structural composites," Proc. of the Fourth Japan-US Conf. on Composite Materials, Technomic Publishing (1989) 981-990.

[78] Y.Q. Ding, W. Wenger and R. MchIlhagger, "Structural characterization and mechanical properties of 3-D woven composites," Proc. of European SAMPE Conf. (1993)

[79] T.R. Guess and E.D. Reedy, "Comparison of interlocked fabric and laminated fabric Kevlar 49/epoxy composites," J.Compos. Technol. & Res., 7 (1985) 136-142.

[80] M. Kotaki and H. Hamada, "Effect of interfacial properties and weave structure on mode I interlaminar fracture behavior of glass satin woven fabric composites," Composites: Part A, 28 (1997) 257-266.

[81] Y. Wang and D. Zhao, "Characterization of interlaminar fracture behavior of woven fabric reinforced polymeric composites," Composites, 26 (1995) 115-124.

[82] R.E. Evans and J.E. Masters, "A new generation of epoxy composites for primary structural applications," ASTM toughened Composite Symposium, (1985)

[83] S.F. Chen and B.Z. Jang, "Fracture Behavior of Interleaved Fiber-Resin Composites," Compos. Sci. & Technol., 41 (1991) 77-97

[84] A. Aksoy and L.A. Carlsson, "Interlaminar shear fracture of interleaved graphite/epoxy composites," Compos. Sci.& Technol., 43 (1992) 55-69.

[85] S.U. Khan and J.K. Kim, “Improved interlaminar shear properties of multiscale carbon fiber composites with bucky paper interleaves made from carbon nanofibers,” Carbon, 50 (2012) 5265-5277.

[86] X. Gong, J. Liu. S. Baskaran, R.D. Voise and J.S. Young, “Surfactant Assisted Processing of Carbon Nanotube/Polymer Composites,” Chem. Mater., 12 (2000) 1049-1052.

[87] B.C. Kim, S.W. Park and D.G. Lee, “Fracture toughness of the nano-particle reinforced epoxy composite,” Compos. Struct., 86 (2008) 69-77.

[88] P. Karapappas, A. Vavouliotis, P. Tsotra, V. Kostopoulos and A. Paipetis,” Enhanced Fracture Properties of Carbon Reinforced Composites by the Addition of multi-wall Carbon Nanotubes,” J. Compos. Mater., 43 (2009) 977-985.

[89] N.R. Mathiavanan and J. Jerald, “Interlaminar Fracture Toughness and Low-Velocity Impact Resistance of Woven Glass Epoxy Composite Laminates of EP3 Grade,” J. Minerals & Materials Characterization & Engineering, 11 (2012) 321-333.

[90] A. Warrier, A.Godara, O. Rochez, L. Mezzo, F. Luizi, L. Gorbatikh, S.V. Lomov, A.W. VanVuure and I. Verpoest, “The effect of adding carbon nanotubes to glass/epoxy composites in the fibre sizing and/or the matrix,” Composites: Part A, 41 (2010) 532-538.

[91] A. Godara, L. Mezzo, F. Luizi, A. Warrier, S.V. Lomov, A.W. van Vuure, L.Gorbatikh, P. Moldenaers and I. Verpoest, “Influence of carbon nanotube reinforcement on the processing and the mechanical behaviour of carbon fiber/epoxy composites,” Carbon, 47 (2009) 2914-2923.

[92] S.C. Joshi and V. Dikshit, “Enhancing interlaminar fracture characteristics of woven CFRP prepreg composites through CNT dispersion,” J. Compos. Mater., (2011) 1-11.

[93] E.J. Garcia, B.L. Wardle and A.J. Hart, “Joining prepreg composite interfaces with aligned carbon nanotubes,” Composites: Part A, 39 (2008) 1065-1070.

[94] E. Bekyarova, E.T. Thostenson, A. Yu, H. Kim, J. Gao, J. Tang, H.T. Hahn, T.W. Chou, M.E. Itkis and R.C. Haddon, “Multiscale Carbon Nanotube – Carbon Fiber Reinforcement for Advanced Epoxy Composites,” Langmuir 23 (2007) 3970-3974.

[95] S.S. Wicks, R.G. de Villoria and B.L. Wardle, “Interlaminar and intralaminar reinforcement of composite laminates with aligned carbon nanotubes,” Compos. Sci. & Technol., 70 (2010) 20-28.

[96] ASTM Standard D5528-01, “Standard test method for Mode I interlaminar fracture toughness of unidirectional fiber-reinforced polymer matrix composite,” West Conshohocken, PA: American Society for Testing and Materials (2007).

[97] JIS K 7086, “Testing methods for interlaminar fracture toughness of carbon fibre reinforced plastics,” Tokyo: Japanese Standards Association, (1993) 651-655.

[98] ASTM Standard D3039/D3039M-08, “Standard Test Method for Tensile Properties of Polymer Matrix Composite Materials,” West Conshohocken, PA: American Society for Testing and Materials (2008).

[99] ASTM Standard D 2344/D 2344M – 00, “Standard Test Method for Short-Beam Strength of Polymer Matrix Composite Materials and Their Laminates,” West Conshohocken, PA: American Society for Testing and Materials (2006).

[100] D.F. Adams and J.M. Busse, “Suggested Modifications of the Short Beam Shear Test Method,” SAMPE, Long Beach Convention Center, Long Beach, CA materials and processing technology, (2004).

APPENDIX

Appendix 1

DCB Specimen Dimensions:

Type of Laminate	Specimen Number	Width b (mm)	Thickness h(mm)	Initial Crack Length a_0 (mm)
Control	1	23.41	4.54	27.16
	2	26.35	4.6	26.89
	3	26.12	4.56	27.01
	4	26.04	4.56	26.92
	5	26.14	4.55	28.27
	6	26.05	4.54	26.42
2 Layers Parallel	1	24.5	4.37	32.47
	2	24.47	4.36	31.22
	3	24.85	4.37	32.01
	4	24.10	4.35	31.36
	5	24.16	4.37	32.33
2 Layers Perpendicular	1	24.09	4.39	32.86
	2	24.04	4.39	32
	3	23.86	4.43	33.86
	4	23.89	4.4	32.17
	5	23.85	4.39	32.16
	6	23.91	4.39	32.06
4 Layers Perpendicular	1	26.32	4.63	28.76
	2	26.29	4.64	28.73
	3	26.23	4.61	28.68
	4	26.27	4.62	28.54
	5	26.27	4.59	27.08
	6	26.35	4.6	29.15
8 Layers Perpendicular	1	26.88	4.6	26.53
	2	26.53	4.59	26.64
	3	26.55	4.6	25.96
	4	26.66	4.58	26.28
	5	26.67	4.58	26.51
	6	26.46	4.59	26.95

ENF Specimen Dimensions:

Specimen Dimensions						
Type	Specimen No.	Half span length L (mm)	Initial crack length a0 (mm)	Width B (mm)	Thickness h (mm)	Length l (mm)
Control	1	50	31.53	25.87	4.42	158
	2	50	30.39	25.66	4.41	158
	3	50	31.58	25.95	4.41	158
	4	50	32.37	25.79	4.38	158
	5	50	32.85	25.5	4.39	158
	6	50	31.09	25.64	4.42	158
2 Layer Perpendicular	1	50	31.91	25.76	4.42	158
	2	50	31.15	25.71	4.39	158
	3	50	31.33	25.93	4.41	158
	4	50	31.84	25.5	4.39	158
	5	50	31.04	25.42	4.37	158
	6	50	31.82	25.85	4.42	158
2 Layer Parallel	1	50	30.97	25.66	4.34	158
	2	50	31.15	25.67	4.33	158
	3	50	31.2	25.54	4.33	158
	4	50	31.41	25.72	4.32	158
	5	50	31.3	25.52	4.34	158
	6	50	31.32	25.66	4.32	158

Tensile Test Specimen Dimensions

Type	Specimen No.	Width B (mm)	Thickness h (mm)	Length L (mm)
Control	1	19.84	2.22	250
	2	20.07	2.22	250
	3	20.1	2.24	250
	4	19.86	2.24	250
	5	19.98	2.24	250
	6	20.16	2.23	250
	7	19.92	2.24	250
2 Layer Perpendicular	1	20.27	2.2	250
	2	19.86	2.22	250
	3	19.86	2.22	250
	4	19.7	2.19	250
	5	19.64	2.2	250
	6	19.75	2.17	250
	7	19.77	2.18	250
2 Layer Parallel	1	2.18	19.57	250
	2	2.2	19.56	250
	3	2.21	19.6	250
	4	2.21	19.44	250
	5	2.21	19.47	250
	6	2.2	19.62	250
	7	2.24	19.47	250

SBS Specimen Dimensions

7 ply CNT modified SBS Specimens				
Type	Specimen No.	Width (mm)	Thickness (mm)	Length (mm)
Control	1	10.6	5.27	53
	2	10.52	5.29	53
	3	10.48	5.27	53
	4	10.51	5.28	53
	5	11.1	5.27	53
	6	11.11	5.26	53
	7	11.13	5.29	53
	8	11.18	5.27	53
Parallel	1	10.55	5.34	52
	2	10.53	5.38	52
	3	10.4	5.35	52
	4	10.58	5.39	52
	5	10.43	5.38	52
	6	10.47	5.33	52
	7	10.52	5.38	52
	8	10.49	5.39	52
Perpendicular	1	10.97	5.3	52
	2	11.12	5.32	52
	3	11.15	5.31	52
	4	11.36	5.34	52
	5	11.3	5.34	52
	6	11.3	5.33	52
	7	11.22	5.35	52

11 ply CNT modified SBS Specimens				
Type	Specimen No.	Width	Thickness	Length
Control	1	10.41	5.23	50
	2	10.55	5.22	50
	3	10.51	5.20	50
	4	10.39	5.22	50
	5	10.39	5.38	50
	6	10.43	5.34	50
	7	10.35	5.39	50
	8	10.56	5.36	50
Parallel	1	10.67	5.26	50
	2	10.41	5.26	50
	3	10.48	5.26	50
	4	10.28	5.25	50
	5	10.44	5.27	50
	6	10.64	5.24	50
	7	10.43	5.26	50
	8	10.56	5.28	50
Perpendicular	1	10.19	5.33	50
	2	10.47	5.33	50
	3	10.45	5.34	50
	4	10.46	5.34	50
	5	10.51	5.30	50
	6	10.52	5.32	50
	7	10.46	5.34	50
	8	10.20	5.34	50

Electrical Resistivity Specimen Dimensions

	Aligned CNT Sheet Direction	Width (mm)	Thickness (mm)	Length (mm)	Cross-Sectional Area (mm^2)
Fiber Direction Long Specimen	Parallel	7.26	2.13	73.82	15.46
	Perpendicular	6.83	2.23	73.81	15.23
Fiber Direction Short Specimen	Parallel	6.89	2.15	57.65	14.81
	Perpendicular	5.99	2.23	57.8	13.35
Through Thickness Direction	Parallel	5.99	2.23	23.93	143.34
	Perpendicular	6.02	2.23	23.27	140.08

Appendix 2

DCB Test Results:

Type of Laminate	Specimen Number	G_{Ic} Initiation Values (kJ/m^2)
Control	1	0.288
	2	0.237
	3	0.283
	4	0.258
	5	0.293
	6	0.221
2 Layers Parallel	1	0.331
	2	0.324
	3	0.342
	4	0.359
	5	0.326
2 Layers Perpendicular	1	0.206
	2	0.277
	3	0.478
	4	0.291
	5	0.31
4 Layers Perpendicular	1	0.149
	2	0.125
	3	0.151
	4	0.146
	5	0.144
	6	0.138
8 Layers Perpendicular	1	0.17
	2	0.109
	3	0.105
	4	0.129
	5	0.140
	6	0.158

ENF Test Results:

G_{IIc} [kJ/m^2]			
Specimen No	Control	2 Layer Parallel	2 Layer Perpendicular
1	0.455	0.381	0.526
2	0.504	0.377	0.527
3	0.387	0.486	0.486
4	0.518	0.465	0.566
5	0.391	0.396	0.585
6	0.549	0.525	0.5965

Tensile Test Results

Type	Specimen No.	Width B (mm)	Thickness h (mm)	P_{max} (N)	F^{tu} (MPa)	E (GPa)
Control	1	19.84	2.22	23378.76	530.527	24.691
	2	20.07	2.22	24989.96	567.375	24.167
	3	20.1	2.24	24853.07	551.996	22.621
	4	19.86	2.24	25008.27	562.155	20.317
	5	19.98	2.24	25042.71	559.548	26.769
	6	20.16	2.23	25432.63	565.712	21.288
	7	19.92	2.24	24409.69	547.047	23.306
2 Layer Parallel	1	20.27	2.2	24411.13	547.408	24.941
	2	19.86	2.22	24291.15	550.954	21.915
	3	19.86	2.22	23640.64	536.200	23.924
	4	19.7	2.19	24405.48	565.68	21.346
	5	19.64	2.2	24381.88	564.290	23.651
	6	19.75	2.17	24528.67	572.330	22.741
	7	19.77	2.18	23415.16	543.292	27.907
2 Layer Perpendicular	1	2.18	19.57	22348.02	523.831	29.699
	2	2.2	19.56	24648.73	572.800	21.849
	3	2.21	19.6	25065.04	578.655	25.678
	4	2.21	19.44	23930.95	557.020	23.403
	5	2.21	19.47	24960.35	580.086	23.174
	6	2.2	19.62	24422.55	565.808	21.835
	7	2.24	19.47	23985.83	549.972	22.422

SBS Test Results

Maximum Load Observed (N) – 7 ply CNT modified laminate			
Specimen	Control	2 Layer Parallel	2 Layer Perpendicular
1	3149.1757	3451.817	3436.9436
2	3266.0292	3437.263	3741.2043
3	3361.854	3344.469	3648.6105
4	3318.2829	3515.619	3749.101
5	3554.8522	3004.078	3671.6804
6	3593.6669	3347.639	3736.8239
7	3464.9538	3585.526	3704.6635
8	3678.9291	3600.51	

Maximum Load Observed (N) – 11 ply CNT modified laminate			
Specimen	Control	2 Layer Parallel	2 Layer Perpendicular
1	3264.998	3296.584	3326.351
2	3241.391	3255.205	3337.681
3	3169.413	3192.718	3360.827
4	3184.625	3068.669	3272.76
5	3358.304	3198.562	3184.224
6	3435.574	3264.71	3343.023
7	3427.447	3359.56	3208.88
8	3414.971	3293.834	3245.833

Short Beam Strength (MPa) – 7 ply CNT modified laminate			
Specimen	Control	2 Layer Parallel	2 Layer Perpendicular
1	42.28	45.95	44.33
2	44.01	45.5	47.43
3	45.65	45.08	46.21
4	44.84	46.23	46.35
5	45.57	40.15	45.63
6	46.12	44.99	46.53
7	44.13	47.51	46.28
8	46.83	47.75	-

Short Beam Strength (MPa) – 11 ply CNT modified laminate			
Specimen	Control	2 Layer Parallel	2 Layer Perpendicular
1	44.97	44.05	45.93
2	44.14	44.58	44.85
3	43.49	43.48	45.16
4	44.03	42.64	43.94
5	45.05	43.6	42.87
6	46.26	43.91	44.79
7	46.07	45.92	43.08
8	45.25	44.3	44.69